J. Fluid Mech. (1974), *vol.* 64, *part* 3, *pp.* 529–563
Printed in Great Britain

Wakes behind two-dimensional surface obstacles in turbulent boundary layers

By J. COUNIHAN,
Central Electricity Research Laboratories, Leatherhead, Surrey
J. C. R. HUNT† AND P. S. JACKSON‡
Department of Applied Mathematics and Theoretical Physics, University of Cambridge

(Received 12 September 1973)

By making simple assumptions, an analytical theory is deduced for the mean velocity behind a two-dimensional obstacle (of height h) placed on a rigid plane over which flows a turbulent boundary layer (of thickness δ). It is assumed that $h \ll \delta$, and that the wake can be divided into three regions. The velocity deficit $-u$ is greatest in the two regions in which the change in shear stress is important, a wall region (W) close to the wall and a mixing region (M) spreading from the top of the obstacle. Above these is the external region (E) in which the velocity field is an inviscid perturbation on the incident boundary-layer velocity, which is taken to have a power-law profile $U(y) = U_\infty(y-y_1)^n/\delta^n$, where $n \ll 1$. In (M), assuming that an eddy viscosity ($= KhU(h)$) can be defined for the perturbed flow in terms of the incident boundary-layer flow and that the velocity is self-preserving, it is found that $u(x, y)$ has the form

$$\frac{u}{U(h)} = -\frac{\tilde{C}}{Kh^2U^2(h)}\frac{f(n)}{x/h}, \quad \text{where} \quad \eta = (y/h)/[Kx/h]^{1/(n+2)},$$

and the constant which defines the strength of the wake is

$$\tilde{C} = \int_0^\infty yU(y)\,(u-u_E)\,dy,$$

where $u = u_E(x, y)$ as $y \to 0$ in region (E).

In region (W), $u(y)$ is proportional to $\ln y$. By considering a large control surface enclosing the obstacle it is shown that the constant of the wake flow is not simply related to the drag of the obstacle, but is equal to the sum of the couple on the obstacle and an integral of the pressure field on the surface near the body.

New wind-tunnel measurements of mean and turbulent velocities and Reynolds stresses in the wake behind a two-dimensional rectangular block on a roughened surface are presented. The turbulent boundary layer is artificially developed by well-established methods (Counihan 1969) in such a way that $\delta = 8h$. These measurements are compared with the theory, with other wind-tunnel measurements and also with full-scale measurements of the wind behind windbreaks.

† Also: Department of Engineering.
‡ Present address: Central Laboratories, Ministry of Works, Lower Hutt, New Zealand.

It is found that the theory describes the distribution of mean velocity reasonably well, in particular the $(x/h)^{-1}$ decay law is well confirmed. The theory gives the correct self-preserving form for the distribution of Reynolds stress and the maximum increase of the mean-square turbulent velocity is found to decay downstream approximately as $(x/h)^{-\frac{3}{2}}$ in accordance with the theory. The theory also suggests that the velocity deficit is affected by the roughness of the terrain (as measured by the 'roughness length' y_0) in proportion to $\ln(h/y_0)$, and there seems to be some experimental support for this hypothesis.

1. Introduction

At present little is known about the wake behind surface obstacles in turbulent boundary layers. This is surprising as there are so many situations in which such flows occur. For example, despite an enormous number of measurements of the wind behind full-scale and model fences and shelter belts there are not even any useful empirical formulae describing the sheltering effects of these obstructions. The most comprehensive review of this subject is the World Meteorological Office (W.M.O.) technical note edited by Eimern *et al.* (1964). A more recent review has been written by Plate (1971*b*).

Flows behind full-scale or model buildings have been investigated much less thoroughly, even though such flows have an important effect on turbulent diffusion from sources in their vicinity (Plate 1967), on the flight of V.T.O.L. aircraft near buildings (Burnham 1967) and on the wind loads on other buildings downwind (Mair & Maull 1971).

In this paper we begin by constructing a simple theory to describe the wakes behind two-dimensional surface obstacles whose height is small compared with the thickness δ of a turbulent boundary layer flowing over the surface. For example, this implies that in the atmosphere the obstacle should be less than about 40 m high. Our method is an adaptation of the theory for the laminar wake behind a two-dimensional obstacle in a laminar boundary layer developed by Hunt (1971*b*). This theory has recently been criticized by Smith (1973), who obtained different expressions for the velocity in the wake well downstream. However, it has been shown by Jackson (1973) that Smith's criticism is only significant far downstream of a body and Hunt's results remain valid for downstream distances not exceeding δ. Jackson has constructed a solution which is uniformly valid and successfully matches the solutions of Smith and Hunt.

Various other approaches have been used in developing theories of two-dimensional wall wakes. The earliest appear to have been those of Tani (1958) and Kaiser (1959), who both modelled a windbreak by a sheet source of (negative) momentum and calculated the wake flow on the assumption that this momentum spread according to the diffusion equation, Tani using a variable and Kaiser a constant diffusion coefficient.† No attempt was made to apply boundary conditions to the velocity deficit at the wall. Sforza & Mons (1970) used similar ideas but made no significant improvements. The most important theory to date is that advanced by Townsend (1965), who was concerned with the effects of

† Another analysis along similar lines is that of Gartshore (1972).

a change in wall boundary conditions on an equilibrium boundary layer. In practice this means that his analysis is only applicable for an obstacle whose height is much less than that of the constant-stress layer. Also the solution is only valid sufficiently far downstream that the obstacle appears as a line singularity on the surface which does not introduce any new length scale of its own. This is a rather serious restriction considering the known effects of separation and reattachment on the length scales of wall turbulence (Bradshaw & Wong 1972).

The region of strong shear near the mean separation streamline is known (see Plate 1971*a*) to be well described by the theory of turbulent mixing layers, but otherwise little is known about the recirculating bubble behind the obstacle.

In a uniform flow the total momentum deficit in the wake of an obstacle is equal to its drag, and consequently several investigations have attempted to find a simple relation for the wake behind an obstacle on a surface. For example, Townsend (1965) postulated some relation of this form to specify the strength of the wake in his theory. A critical review of the various attempts to relate the integral of the momentum deficit in the wake to the drag has recently been given by Seginer (1972). Using Nageli's (1953) detailed experimental data for the horizontal component of velocity in the wake of a fence, Seginer calculated each term of the momentum integral. He was able to show which terms were the most important but did not find any connexion between the drag on the obstacle and the momentum deficit in its wake.

Existing computational methods for calculating turbulent boundary layers are not applicable to this problem, because the obstacle introduces length and velocity scales which are not characteristic of boundary layers and so cannot be specified in advance. But it would be interesting to see the computational methods for solving elliptic problems, outlined by Launder & Spalding (1972), being applied to this problem.

The primary object of the present theory is to predict as simply as possible, and without extensive computation, the properties of the velocity deficit and, if possible, the shear stress and turbulence in the wake. This has required an over-simple assumption about the relation between shear stress and mean velocity gradients, but the satisfactory agreement of the analysis with experiments appears to justify its use. A more elaborate theory, perhaps involving the solution of the turbulent energy equation (Bradshaw, Ferriss & Atwell 1967; Townsend 1961), may be worth developing in the future.

A second aim of the theory is to relate the velocity deficit in the wake to the forces on the obstacle, by analogy with the relation between the total momentum deficit and the drag in the wake behind a body in a uniform flow. Such a relation, for certain types of obstacle, was obtained by Hunt (1971*b*), linking an integral of the velocity deficit indirectly to the *couple* on the obstacle. In the theory presented here it is found that a certain integral of the velocity which is constant along the wake is related to the pressure field on the body and on the surface near the body, but there is no direct relation with the couple.

There have been many measurements of wakes behind two-dimensional surface obstacles in turbulent boundary layers both in wind tunnels and in the natural

wind. A review has been made recently by Plate (1971*a*). However, the purpose of these measurements has usually been practical rather than scientific and in particular no detailed turbulence measurements behind a two-dimensional obstacle on an aerodynamically rough surface have been published. Plate & Lin (1965) made detailed measurements on a smooth wall of the mean and r.m.s. turbulent velocities behind two-dimensional wedges which were smaller than the boundary-layer thickness. Good & Joubert (1968) have made the most detailed measurements of pressure and drag on two-dimensional fences with various heights, but they only measured the flow field for a particular fence, which was higher than the boundary-layer thickness. Other wind-tunnel studies are mentioned later. The only comprehensive full-scale measurements are those made by Nageli (1953) of wind behind 2·2 m high fences in Switzerland. Even then only mean velocities were measured, though comments were made about the turbulence.

The experiments described in § 3 of this paper were performed in a wind tunnel at the Central Electricity Research Laboratories. A two-dimensional obstacle was placed in a turbulent boundary layer over a rough wall. The boundary layer, which was artificially thickened, was an accurate simulation of the atmospheric boundary layer (Counihan 1969). Mean and fluctuating velocities and Reynolds stresses were measured, and thus a comprehensive description of the wake is possible. The results generally agree with our simple theory. In § 4, we also compare the results of our theory with the wind-tunnel experiments of Plate & Lin (1965) and with the full-scale measurements of Nageli (1953). We also compare our experimental results with these previous experiments. Some general conclusions are drawn in § 5.

Some of the results of this paper were briefly mentioned in a review paper by Hunt (1971*a*). The theory presented here is the work of Hunt and Jackson and the experiments were performed by Counihan.

2. Theory of two-dimensional wakes

2.1. *Assumptions*

Our analysis for the flow over a rough surface behind a two-dimensional body in a turbulent boundary layer is based on a number of assumptions, which will be described with reference to figure 1.

(I) If k, h and δ are respectively the heights of the roughness elements in the incident boundary layer, the body whose wake is to be studied and the boundary layer, then we assume

$$k \ll h \ll \delta. \tag{2.1}$$

In addition the shape of the obstacle must be such as to cause a well-defined turbulent separation bubble in its lee.

(II) Sufficiently far downstream ($x > X$), but in a distance less than that (L) which it takes for the velocity in the undisturbed boundary layer to change appreciably, we assume that the mean velocity in the wake $(\overline{u}_x(x, y), \overline{u}_y(x, y), 0)$ returns to its value in the undisturbed boundary layer, defined as $(U(y), V(y), 0)$.

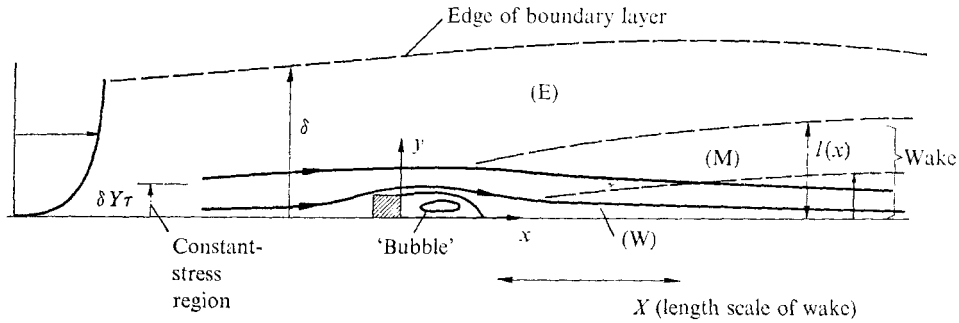

FIGURE 1. A two-dimensional surface obstacle in a turbulent boundary layer showing the regions of flow and two typical streamlines.

This assumption has been used to described laminar wakes by Hunt (1971*b*) and for laminar wakes has been given a formal justification by Jackson (1973). In the case of a turbulent boundary layer this assumption is more generally valid because the large eddies in the outer part of the boundary layer can diffuse the momentum deficit in the wake more efficiently than purely viscous shear stresses. The implication of this assumption is that there is a range of values of $x < X$ within which $|\overline{u}_x(x,y) - U(y)|$ is small compared with $U(y)$.

(III) The main assumption about the upstream boundary layer is that the mean velocity profile can be described by a power law (Plate 1971*b*),

$$U(y) = U_\infty[(y-y_1)/\delta]^n, \tag{2.2}$$

where U_∞ is the wind speed outside the boundary layer. The exponent n is chosen to obtain the best fit over the lower part of the boundary layer where the wake develops. This profile cannot hold very close to the roughness elements (where $y \simeq k$), when a logarithmic profile becomes a better description:

$$U(y) = \frac{U_*}{\kappa} \ln\left(\frac{y-y_1}{y_0}\right), \tag{2.3}$$

where $\kappa (= 0{\cdot}4)$ is von Kármán's constant. For $y < k$, a new description for the profile is needed which is of no consequence for our analysis. The parameter y_1, a 'zero-plane displacement' for the incident boundary layer, has to be incorporated in (2.2) to describe the velocity profile satisfactorily; the relation between y_0 and k depends on the density of roughness elements, but it is usually found that y_0 is of order $0{\cdot}15k$. For the logarithmic profile y_0 is the 'roughness length'.

It is useful to note that for most zero-pressure-gradient turbulent boundary layers the mean turbulent shear stress $\overline{\tau}_{xy}$ is approximately constant for $y/\delta < Y_\tau$, where $Y_\tau \simeq 0{\cdot}15$. U_* is defined in terms of $\overline{\tau}_{xy}$ as $U_* = (\overline{\tau}_{xy}/\rho)^{\frac{1}{2}}$.

(IV) Far downstream of the body the small perturbations to the incident flow caused by the body can be divided into three regions. The region downstream of the body adjacent to the rough wall is denoted as the wall region (W) and is assumed to be an 'equilibrium' layer in the sense of Townsend (1961). Turbulent energy production locally balances dissipation, and with additional physically plausible (and by now well-established) assumptions the perturbation shear

stress and velocity profile can be calculated. It is assumed that this region has a thickness $y_\tau(x)$ which necessarily is less than Y_τ. Since $y_\tau(x)$ increases downstream this assumption imposes an upper limit on the values of x for which the theory is valid.

Also, downstream of the body, above (W), we postulate the existence of a mixing region (M) with a depth of order $l(x)$, where $l(x) \ll X$, X being a distance characteristic of the length of the wake. In this zone, where inertial and shear stresses balance, we assume that the shear layer shed from the body, the turbulence transported from the wall and the turbulence convected from the upstream flow produce a perturbation flow which is self-preserving, i.e. one in which "motions at different sections differ only in velocity and length scales, and are dynamically similar in those aspects of motion controlling mean velocity and Reynolds stress" (Townsend 1956). The reason for this assumption is that there are no length scales imposed on the flow other than the height of the obstacle. This is because the flow is independent of fluid viscosity if $|\bar{u}_x|\, l/\nu \gg 1$ and because, even though $U(y) = (U_1/\delta^n)\, y^n$, δ is not a relevant length scale when $h \ll \delta$. Thus the length scales are the height of the body h and the intrinsic dimensions $l(x)$ and X. Since $l \ll X$, in regions (M) and (W) $\partial/\partial y \gg \partial/\partial x$. The obstacle and the mixing zone (M) create a third disturbed region (E), which is an inviscid perturbation on the boundary-layer flow. In this region, which may or may not penetrate beyond the boundary layer, $\partial/\partial x \sim \partial/\partial y$.

Thus in regions (M) and (E)

$$\bar{u}_x = u(x,y) + U(y), \quad \bar{u}_y = v(x,y) + V(y), \tag{2.4}$$

where $|u|, |v| \ll U(y)$, and in (M) $u(x,y)$ and $v(x,y)$ have self-preserving forms. The orders of magnitude of v and V follow from continuity, namely,

$$\left.\begin{aligned} v &\sim ul/X, \quad V \sim Ul/L \quad \text{in (M),} \\ v &\sim u, \qquad V \sim U\delta/L \quad \text{in (E).} \end{aligned}\right\} \tag{2.5}$$

Note that this particular division of the flow into zones is entirely dependent on our first assumption that $h \ll \delta$. It somewhat differs from the analytically imprecise divisions of Plate (1971*a*), which appear to describe wakes for all ratios h/δ of the height of the body to that of the boundary layer. A further detailed assumption (V) about matching the two regions (M) and (W) is described in § 2.2.

2.2. *Calculations of mean velocities*

The time-averaged equations for the rate of change of momentum and for continuity in a steady turbulent flow are

$$\bar{u}_x \frac{\partial \bar{u}_x}{\partial x} + \bar{u}_y \frac{\partial \bar{u}_x}{\partial y} = \frac{1}{\rho}\left\{ -\frac{\partial \bar{p}}{\partial x} + \frac{\partial \bar{\tau}_{xy}}{\partial y} + \frac{\partial \bar{\tau}_{xx}}{\partial x} \right\}, \tag{2.6}$$

$$\bar{u}_y \frac{\partial \bar{u}_y}{\partial y} + \bar{u}_y \frac{\partial \bar{u}_y}{\partial y} = \frac{1}{\rho}\left\{ -\frac{\partial \bar{p}}{\partial y} + \frac{\partial \tau_{xy}}{\partial x} + \frac{\partial \bar{\tau}_{yy}}{\partial y} \right\}, \tag{2.7}$$

$$\partial \bar{u}_x/\partial x + \partial \bar{u}_y/\partial y = 0, \tag{2.8}$$

where $\overline{\tau}_{xx}$, $\overline{\tau}_{xy}$ and $\overline{\tau}_{yy}$ are the combined Reynolds and viscous stresses and $\overline{p}$ is the mean pressure. On substituting the expressions for $\overline{u}_x$ and $\overline{u}_y$ from (2.4) into (2.6) and (2.7), and using the order-of-magnitude estimates for v and V in (2.5), it follows that the terms in V can be ignored. Therefore the velocity components in the wake regions can be expressed as

$$\overline{u}_x = u(x,y) + U(y), \quad \overline{u}_y = v(x,y), \tag{2.9}$$

where $|u|, |v| \ll U(y)$. It follows from this assumption that

$$\overline{p} = p(x,y) + P(x,y) \tag{2.10}$$

and

$$\overline{\tau}_{xx} = \tau_{xx} + T_{xx}, \quad \text{etc.}, \tag{2.11}$$

where $P(x,y)$, T_{xx}, etc., are the mean stresses in the undisturbed boundary layer. Substituting (2.9)–(2.11) into (2.6)–(2.8) and eliminating the terms for the undisturbed boundary layer, we obtain the following equations for the perturbation quantities:

$$U(y)\frac{\partial u}{\partial x} + v\frac{\partial U}{\partial y} = \frac{1}{\rho}\left\{-\frac{\partial p}{\partial x} + \frac{\partial \tau_{yx}}{\partial y} + \frac{\partial \tau_{xx}}{\partial x}\right\}, \tag{2.12}$$

$$U(y)\frac{\partial v}{\partial x} = -\frac{1}{\rho}\frac{\partial p}{\partial y} + \frac{1}{\rho}\frac{\partial \tau_{yy}}{\partial y}, \tag{2.13}$$

$$\partial u/\partial x + \partial v/\partial y = 0. \tag{2.14}$$

Mixing region (M). To specify the problem completely the perturbation stresses τ_{xy}, etc., have to be related to the perturbation mean velocities. These relations are different in (M) and (W). The assumption that the flow in region (M) is self-preserving does not determine the relation between τ_{xy} and $u(x,y)$. As we have set out to achieve a simple model of the wake we consider the simplest relation, namely

$$\overline{\tau}_{xy} = \rho \nu_M \, \partial \overline{u}_x / \partial y,$$

where ν_M is the eddy viscosity.

The change in stress arising from an additional rate of strain cannot be found unless the effect of the strain on the eddy viscosity is known. Bradshaw (1971) expressed this effect by

$$\nu_M = \nu_0\left[1 + a\frac{\partial u/\partial y}{dU/dy} + b\frac{\partial v/\partial x}{dU/dy}\right],$$

where ν_0 is the eddy viscosity of the undisturbed boundary layer and a and b are constants. We shall assume that ν_M depends linearly on $\partial \overline{u}_x/\partial y$, so that $a = 1$. Bradshaw (1971) and Townsend (1972) have both noted that the strain $\partial v/\partial x$ has a strong effect on the eddy viscosity and estimated that $b \simeq 10$, but it is nevertheless negligible in the expression above if l/X is sufficiently small that $3l \ll X$. Thus, in the mixing region, the perturbation stress τ_{xy} is given by $\tau_{xy} = 2\nu_0(y)\,\partial u/\partial y$. Since the upstream flow, including the large eddies of the outer boundary layer, has been mixed by the flow over the body, it seems appropriate to take an average value of ν_0 to estimate the shear stress in the wake, say ν_0 at the height of the body $y = h$. In some respects the mixing region (M) might

be expected to resemble a turbulent wake in a uniform flow, where many observations confirm that $\bar{\tau}_{xy} \propto \partial \bar{u}_x/\partial y$. For these reasons we *assume* that in (M)

$$\tau_{xy} = \rho 2\nu_0(y = h)\,\partial u/\partial y, \tag{2.15}$$

where, by definition, $\nu_0(y = h) = T_{xy}/(dU/dy)$. If the obstacle lies within the constant-stress layer of the incident flow, $\nu_0(h)$ may be found using the usual mixing-length expression

$$U_*^2 = T_{xy}/\rho = \kappa^2 y^2 (dU/dy)^2 = \nu_0\, dU/dy, \tag{2.16}$$

that is,

$$\nu_0(h) = \kappa h U_*. \tag{2.17}$$

If the components of the perturbation stress are all of the same order of magnitude the equation of motion (2.12) now becomes, for $y \gg y_1$,

$$U_\infty \left(\frac{y}{\delta}\right)^n \frac{\partial u}{\partial x} + U_\infty n \left(\frac{y}{\delta}\right)^{n-1} \frac{v}{\delta} = -\frac{1}{\rho}\frac{\partial p}{\partial x} + 2\nu_0(h)\frac{\partial^2 u}{\partial y^2}. \tag{2.18}$$

While the displacement height y_1 is a useful device for fitting (2.2) to a turbulent boundary layer, it is not obvious that the wake will experience the same displacement. As a first approximation, therefore, it has been omitted from (2.18), which means that the solution of this equation will not be valid when $y \sim y_1$; this is of no consequence because we have already postulated that it only holds in the region (M), well away from the wall.

The proposed solution is

$$\left.\begin{aligned} \frac{u}{U(h)} &= \frac{\hat{u}}{\bar{x}^m}\frac{df}{d\eta}, \\ \frac{v}{U(h)} &= \frac{\hat{u}}{\bar{x}^{m+1}}\left[mf - \frac{\bar{x}}{l}\frac{dl}{d\bar{x}}(f - \eta f')\right]\left(\frac{l}{h - y_1}\right), \\ \frac{p}{\rho U^2(h)} &= \frac{\hat{u} p_0}{\bar{x}^m}\left(\frac{l}{h - y_1}\right)^n, \end{aligned}\right\} \tag{2.19a}$$

where $\bar{x} = x/(h - y_1)$ and $\eta = y/l(\bar{x})$. $f(\eta)$ is assumed to be $O(1)$, so that $\hat{u}$ specifies the magnitude of the velocity deficit in the wake. The form for u is suggested by the type of function known to describe other self-preserving flows, such as jets and wakes. The expression for v is then chosen to satisfy continuity. The length $h - y_1$ is the only reference length available well away from the wall, hence the definition of $\bar{x}$.

Substituting (2.19*a*) into (2.18), it is found that this self-preserving solution may exist only if

$$l/(h - y_1) = (K\bar{x})^{1/(n+2)},$$

where

$$1 \ll K^{-1} = \frac{(h - y_1)\,U(h)}{2\nu_0(h)} \simeq \frac{U(h)}{2\kappa U_*} = \frac{\ln[(h - y_1)/y_0]}{2\kappa^2}. \tag{2.19b}$$

Hence the rate of spread of the wake is found to depend only on the parameter K, which can be regarded as a measure of the ratio of shear stresses to inertial stresses (i.e. a turbulent 'Reynolds number' of the obstacle). K is also a measure of the roughness height of the surface relative to the height of the obstacle. In

Townsend's (1965) analysis only the roughness height y_0 occurs in the analysis. The height of the obstacle does not, which is why Townsend's analysis can only be valid very far downstream of the obstacle, even if the other condition that $h \ll Y_\tau$ is satisfied.

The differential equation for $f(\eta)$ is then

$$(n+2)f''' + \eta^{n+1}f'' + [m(n+2)-n]\eta^n f' + n[1-m(n+2)]\eta^{-1}f = m(n+2)p_0. \tag{2.20}$$

Only two boundary conditions are available at the wall, so at least one solution must be eliminated by considering the limit $\eta \to \infty$. The asymptotic behaviour of the solutions is

$$f \sim \eta^n, \quad \eta^{1-m(n+2)}, \quad p_0\eta^{1-n}.$$

The first corresponds to a simple displacement of the velocity profile (i.e. $u \propto dU/dy$), which is quite permissible. The second implies that at the edge of the wake u does not tend to zero, in fact it becomes independent of x. As this is a boundary-layer profile rather than a wake profile this solution is omitted. The remaining term is the particular integral representing a coupling via the perturbation pressure between the wake and the flow in the outer region (E). From the subsequent analysis of the external region (E) it follows that if

$$n(1-n)/l^2(x) \gg x^{-2},$$

which should be satisfied in most turbulent wakes, the pressure term is zero and the appropriate behaviour as $\eta \to \infty$ is evidently $f \sim \eta^n$.

Two solutions have this behaviour, and there are two wall conditions remaining. The appropriate solution cannot be determined until m is found, which is usually achieved using a conservation condition for some physical quantity in the wake. We write

$$u = u_E(x,y) + \tilde{u}(x,y), \quad v = v_E(x,y) + \tilde{v}(x,y),$$

where

$$u_E = A(x)\,dU/dy, \quad v_E = -U(y)\,dA/dx.$$

u_E and v_E are the solutions for region (E) as $y \to 0$ and are the leading terms in the expansions of u and v in terms of η as $\eta \to \infty$. On substituting into (2.18) (but now omitting the pressure gradient), multiplying by y, integrating from y_τ to ∞ and using the continuity equation, we find

$$\frac{U(h)}{h^n}\frac{1+2n}{1+n}\int_{y_\tau}^{\infty} y^{n+1}\frac{\partial \tilde{u}}{\partial x}\,dy = \left[\frac{U(h)\,n y^{n+1}}{1+n\,h^n}\tilde{v} + KhU(h)\left(u - y\frac{\partial u}{\partial y}\right)\right]_{y=y_\tau}. \tag{2.21}$$

If the analysis for (M) were valid down to the surface, i.e. $y_\tau \to 0$, where $u, \tilde{v} = 0$, then the right-hand side would be zero and

$$\int_0^{\infty} y\,U(y)\,\tilde{u}\,dy = -\tilde{C}, \tag{2.22}$$

where $\tilde{C}$ is a constant. In fact $y_\tau \neq 0$, and in the wall region ($y < y_\tau$) the expression for the shear stress is different, so that the result (2.22) is not exact. However, it can be shown from the solution for (u, v) in (W) that the error in (2.22) caused by

ignoring the wall region (W) is small. The self-preserving solution can only satisfy the conservation condition (2.22) if $m = 1$, when

$$\int_0^\infty \eta^{1+n}\,[f' - \lim_{\eta\to\infty} f']\,d\eta = I,$$
$$I = -\tilde{C}/K(h-y_1)^2\,U^2(h)\,\hat{u}. \tag{2.23}$$

The appropriate solution to (2.20) is found by multiplying through by η and integrating from η to ∞. Then

$$f(\eta) = f_1(\eta) + Bf_2(\eta), \tag{2.24}$$

where

$$f_1(\eta) = \eta^2\,{}_1F_1\left(\frac{2-n}{2+n}, \frac{4+n}{2+n}, \frac{-\eta^{2+n}}{(2+n)^2}\right),$$

$$f_2(\eta) = {}_1F_1\left(\frac{-n}{2+n}, \frac{n}{2+n}, \frac{-\eta^{2+n}}{(2+n)^2}\right),$$

${}_1F_1$ is the confluent hypergeometric function defined by Abramowitz & Stegun (1964, p. 504) and B is a constant. Note that, as $\eta \to 0, f_1 \sim \eta^2, f_2 \sim 1 + O(\eta^{2+n})$ and both f_1 and f_2 increase like η^n as $\eta \to \infty$. The choice of the appropriate constants for f_1 and f_2 is fixed by the conservation condition (2.23) and by matching the solutions for u, v and τ_{xy} at the boundary between regions (M) and (W). From the solution in region (W) it follows that this matching condition fixes B, which is found to be $O(1)$. Since the functions in (2.24) are such that $f_1' \gg f_2'$ when $\eta \gtrsim 1$, $u(x, y)$ may be expressed solely in terms of f_1'.

When $n = 0$, $f_1' = 2\eta e^{-\frac{1}{4}\eta^2}$, which gives the general shape of the velocity profile for small n. The exact profile is insensitive to the particular value of n, for $n \ll 1$.

In order to express the wake strength $\hat{u}$ in terms of the constant $\tilde{C}$, the integral I is needed. It is found to be (when $B = O(1)$)

$$I(n) = \frac{(1+n)\,(2+n)^{(4+n)/(2+n)}}{1+2n}\,\frac{\Gamma\left(\frac{4+n}{2+n}\right)\Gamma\left(\frac{1-n}{2+n}\right)}{\Gamma\left(\frac{2-n}{2+n}\right)}. \tag{2.25}$$

Typical values are $I = 7{\cdot}08$ for $n = 0$, $7{\cdot}95$ for $n = 0{\cdot}2$. The final expression for the velocity deficit is

$$\frac{u}{U(h)} = -\frac{\tilde{C}/I(n)}{K(h-y_1)^2\,U^2(h)}\left(\frac{h-y_1}{x}\right)\frac{d}{d\eta}\left[\eta^2\,{}_1F_1\left(\frac{2-n}{2+n}, \frac{n+4}{2+n}, \frac{-\eta^{n+2}}{(n+2)^2}\right)\right]. \tag{2.26}$$

An implication of this expressionis that, if $\tilde{C}/[(h-y_1)^2\,U^2(h)]$ depends mainly on the obstacle geometry, the velocity deficit is approximately inversely proportional to K. Since K increases with increasing surface roughness, the wake strength then decreases as y_0 increases.

One particular velocity profile is shown in figure 2 (*a*) with a value of $\tilde{C}$ appropriate to the experiments described later.

Wall region (W). The earlier approximation that ν_0 is constant must be very poor near the wall, where one expects the velocity profile to be logarithmic, or

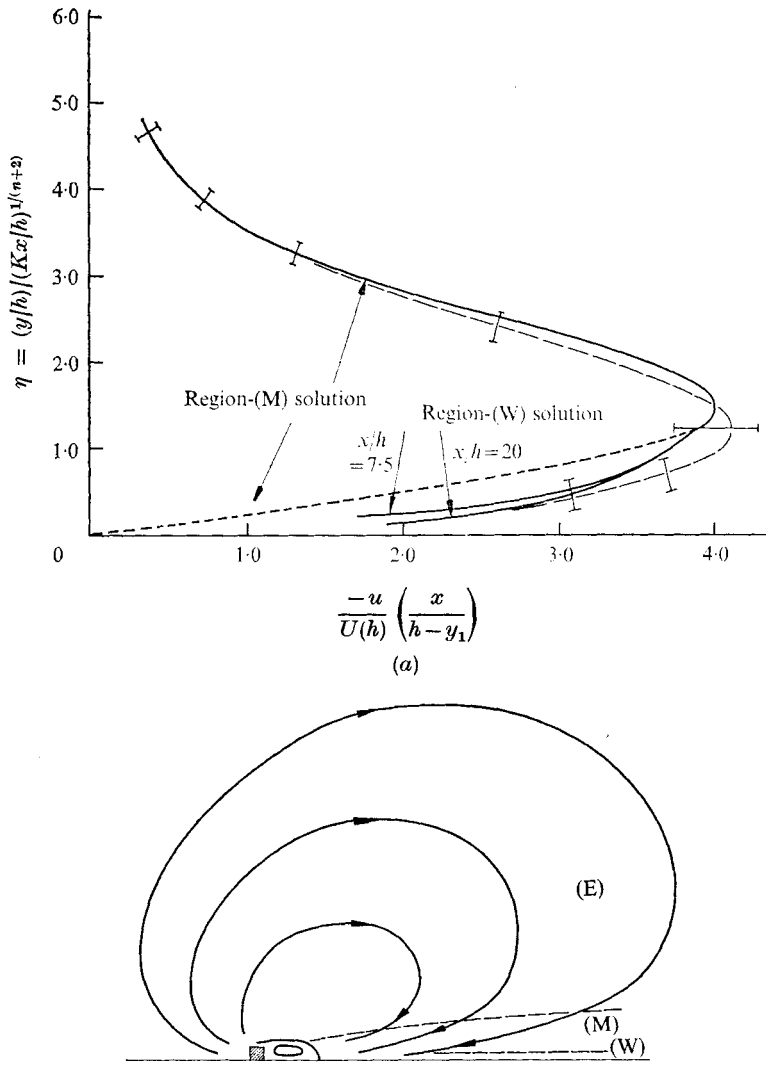

FIGURE 2. The wake of a two-dimensional obstacle. (*a*) Self-preserving velocity profile in regions (M) and (W). —I—, experimental curve with scatter bar ($n = 0{\cdot}125$, $h/\delta = \frac{1}{8}$); ——, theoretical curve (magnitude chosen to give best fit with experimental profile at maximum); – – – –, extrapolation of region-(M) solution into region (W). (*b*) Perturbation streamlines of the wake flow in regions (E), (M) and (W).

$\nu_0 \propto y$. Since we have shown that the perturbation pressure gradient $-\partial p/\partial x$ is negligible, and since $u, v \to 0$ as $y \to 0$ in the wall region, the momentum equation requires that close to the wall $\partial \tau_{xy}/\partial y = 0$. From the arguments of Townsend (1961) and our assumption that the wall region is in equilibrium it follows that near $y = 0$ the *total* velocity is

$$\overline{u}_x = \left(\frac{\overline{\tau}_{xy}}{\rho}\right)^{\frac{1}{2}} \frac{1}{\kappa} \ln \frac{y - y_1}{y_0}, \tag{2.27}$$

where $(\bar{\tau}_{xy}/\rho)^{\frac{1}{2}} = U_* + F(\bar{x})\,u_*$. Therefore as $y \to 0$ the perturbation velocity is

$$u = \frac{u_* F(\bar{x})}{\kappa} \ln \frac{y - y_1}{y_0}, \tag{2.28}$$

where u_* and $F(\bar{x})$ are unknown functions. The result (2.28) cannot be valid throughout the wall region (W), because the shear stress τ_{xy} must vary with y to balance the inertial stresses, which grow from zero at the wall to their value in the mixing region at $y = y_\tau(x)$. Since we have not obtained a complete solution for this region, we adopt (2.28) as an approximation to u for the whole wall region $0 < y < y_\tau(x)$. Then u_* and $F(\bar{x})$ are determined by matching u and τ_{xy} with solutions in (M) at $y_\tau(x)$. The vertical velocity v may be matched by calculating v from (2.28) and matching with v in (M), which has to be calculated using both expressions f_1 and f_2 in (2.24).

The eddy viscosity (and hence velocity gradient) is discontinuous between (W) and (M) if (2.27) is assumed to hold throughout (W); this must be accepted in the interests of simplicity, but it is encouraging that Bradshaw & Wong (1972) have reported finding just such a discontinuity in a numerical study of this problem. The matching conditions at $y = y_\tau$ give

$$\frac{u_* F(\bar{x})}{\kappa} \ln \frac{y_\tau - y_1}{y_0} = \frac{\hat{u}}{\bar{x}} f'(y_\tau/l)\, U(h) \tag{2.29}$$

and

$$2U_* u_* F(\bar{x}) = \frac{2\hat{u}\nu_0(h)}{\bar{x}l} f''(y_\tau/l)\, U(h). \tag{2.30}$$

These lead to complicated expressions for u_*, $F(\bar{x})$ and y_τ unless $\eta_\tau = y_\tau/l$ is close to the value of η at which $f''(\eta)$ vanishes. This assumption is confirmed by the solution below. Then writing

$$\eta_\tau = \eta_0 + \epsilon, \quad \text{where} \quad |\epsilon| \ll \eta_0, \tag{2.31}$$

substituting into (2.29) and (2.30) and omitting terms in ϵ^2, we find

$$\epsilon = \frac{\kappa U_* l}{\nu_0(h)} \frac{f'(\eta_0)}{f'''(\eta_0)} \left[\ln\left(\frac{\eta_0 l - y_0}{y_0}\right)\right]^{-1}. \tag{2.32}$$

Using $\nu_0(h) \doteq \kappa h U_*$, it is clear that ϵ is small when $l \sim h \gg y_0$. The velocity deficit is now

$$\frac{u}{U(h)} = \frac{\hat{u}}{\bar{x}} f'(\eta_0) \frac{\ln[(y - y_1)/y_0]}{\ln[(\eta_0 l - y_1)/y_0]} \simeq \frac{\hat{u}}{\bar{x}} f'(\eta_0) \left[\frac{\ln \eta + \ln(l/y_0)}{\ln \eta_0 + \ln(l/y_0)}\right], \tag{2.33a}$$

which is similar to the solution obtained by Townsend (1965). To the same approximation the change in stress is

$$\tau_{xy} = \frac{2\rho U(h)\, U_* \kappa \hat{u} f'(\eta_0)}{\bar{x} \ln[(\eta_0 l - y_1)/y_0]}. \tag{2.33b}$$

The solutions (2.33*a*, *b*) are strictly only valid as $y \to 0$, because inertial effects have been ignored in their derivation. However, as we shall see in § 3, these results describe the velocity profiles well and give a stress with the correct order of magnitude near $y = 0$.

External flow region (E). The governing equation for region (E) is obtained by taking the curl of the momentum equations (2.12) and (2.13), omitting the shear stress terms, and using the continuity equation (2.14) to express u in terms of v. Then, expressing $U(y)$ in its power-law form from (2.2) and using the fact that $y \gg y_1$ in region (E), we find that

$$\frac{\partial^2 v}{\partial x^2} + \frac{\partial^2 v}{\partial y^2} + \frac{n(1-n)}{y^2} v = 0.$$

Consider the order of magnitude of the various terms in this equation when $y \sim l(x)$, i.e. near the boundary between regions (E) and (M). It follows from the self-preserving form of v in region (M) that, whatever the precise asymptotic form of $f(\eta)$, as $\eta \to \infty$, $\partial^2 v/\partial x^2 = O(v/x^2)$. Thence, if x is sufficiently large that $n(1-n)/l^2 \gg x^{-2}$, we can assume that, in the lower part of (E),

$$\partial^2 v/\partial x^2 \ll n(1-n)\, v/y^2.$$

Thus the governing equation becomes $\partial^2 v/\partial y^2 + n(1-n)\, v y^{-2} = 0$, whose solution is

$$v = -\frac{U_\infty}{\delta^n} \frac{dA}{dx} y^n = -\frac{dA}{dx} U(y),$$

and by continuity

$$u = (U_\infty/\delta^n)\, A(x)\, n y^{n-1} = A(x)\, dU/dy.$$

If these expressions are substituted into (2.12), omitting the shear stress terms, then we find that, in this lower part of (E), $\partial p/\partial x = 0$. This explains the choice for the asymptotic form of $f(\eta)$ and why the perturbation pressure term p_0 can be neglected. In the outer part of (E), where $\partial^2 v/\partial x^2$ cannot be neglected, $v(x, y)$ has a different form and a second-order pressure gradient is induced. The wake of a small obstacle in a constant-pressure laminar boundary layer is quite different from that in a turbulent boundary layer because near the wall $\partial^2 U/\partial y^2 \simeq 0$, so that throughout (E) $\partial^2 v/\partial x^2$ is of the same order as $\partial^2 v/\partial y^2$. Then a first-order perturbation pressure is induced by the vertical flow into the wake (Hunt 1971*b*). However, even in a laminar wake sufficiently far downstream that $x \sim \delta$, when the depth of the wake $l(x)$ extends into the upper part of the boundary layer where the velocity profile is no longer linear, in the lower part of region (E) $\partial^2 v/\partial x^2$ becomes negligible and the vertical velocity component takes the form $v = -A'(x)\, U(y)$ and p becomes negligible (Smith 1973; Jackson 1973).

Streamlines for regions (W), (M) and (E) are sketched in figure 2(*b*), which shows how the flow in the outer part of the boundary layer resembles that over a long obstacle on the surface. The flow in the lower part of (E) is a pure displacement of the undisturbed flow. The overall pattern of the streamlines is similar to that for a laminar wake given by Hunt (1971*b*) despite the differences between laminar and turbulent wakes.

2.3. *Relations between the forces on the body and the flow in its wake*

For a body placed in a uniform flow the relation between the wake strength and the drag D on the obstacle is quite simple, namely

$$D = -\rho \int_{-\infty}^{\infty} U u \, dy.$$

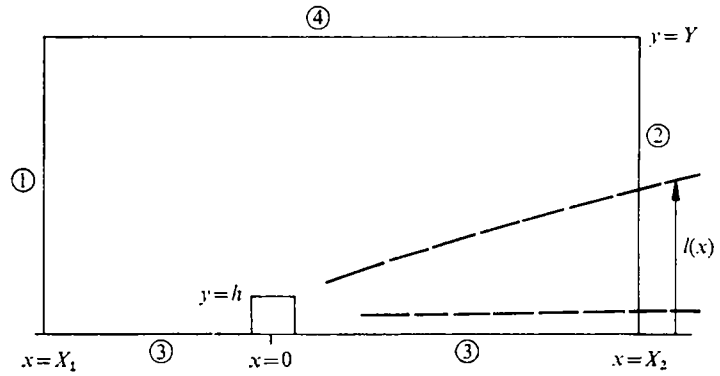

FIGURE 3. Control surface for evaluating the relation between forces on a two-dimensional obstacle and the flow in the wake.

However, the relation for an obstacle placed on (or near) a rigid surface may not be so simple because of the change in shear stress on the surface. Consider the control surface, shown in figure 3, with faces 1 and 2 at $x = X_1$, X_2 and faces 3 and 4 at $y = 0$, Y. Denoting a particular face by a suffix, the momentum balance is

$$D/\rho = \int_0^Y \left\{\frac{\bar{p}_1 - \bar{p}_2}{\rho} + \bar{u}_{x_1}^2 - \bar{u}_{x_2}^2 - \frac{1}{\rho}(\bar{\tau}_{xx_1} - \bar{\tau}_{xx_2})\right\} dy - \int_{X_1}^{X_2} \frac{1}{\rho}(\bar{u}_{x_4}\bar{u}_{y_4} - \bar{\tau}_{xy_4})\, dx - \frac{1}{\rho}\int_{X_1}^{X_2} \bar{\tau}_{xy_3}\, dx.$$

If X_1 is taken far upstream and X_2 is chosen to lie in that part of the wake where the analysis of § 2.2 holds ($L \gg X_2 \gg h$ and $\delta \gg Y \gg l(X_2)$, then subtracting the terms for the undisturbed flow and neglecting the higher-order terms in the wake which include the perturbation pressure p

$$D = -\rho\int_0^Y 2U(y)\, u(X_2, y)\, dy - \rho\int_{-\infty}^{X_2} U(Y)\, v(x, Y)\, dx - \int_{-\infty}^{X_2} \tau_{xy}(x, 0)\, dx.$$

Using continuity

$$D + \int_{-\infty}^{X_2} \tau_{xy}(x, 0)\, dx = -\rho\int_0^Y [2U(y) - U(Y)]\, u(X_2, y)\, dy. \tag{2.34}$$

Substituting the expression found earlier for u, one finds that as the control volume expands

$$\lim_{X_2 \to \infty} \left\{D + \int_{-\infty}^{X_2} \tau_{xy}(y = 0)\, dx\right\} = 0, \tag{2.35}$$

that is, the drag on the obstacle exactly balances the total change in drag on the wall. An implication of (2.35) is that

$$\int_{-\infty}^{\infty} \tau_{xy}(y = 0)\, dx$$

is a convergent integral. This is surprising since it follows from (2.34) that $\tau_{xy}(y = 0) \sim (x \ln x)^{-1}$. But (2.34) is only valid if $l(x) \sim h$, and further downstream

where $l(x) \gg h$, it can be shown that asymptotically $\tau_{xy}(y=0) \sim x^{-\frac{3}{2}}$. Consequently (2.35) is a correct statement within the context of our assumptions. The result (2.35) is unlikely to apply to most experiments with finite values of h/δ because, over the length of the wake, the profile of the incident boundary-layer flow does not remain constant. Also we have assumed that, to first order in $\hat{u}/U(h)$, $u \to 0$ as $x \to \infty$, whereas it is observed that the development of a boundary layer is to a small extent permanently changed by a small surface obstacle. This implies that, to second order in $\hat{u}/U(h)$, it is likely that $u \neq 0$ as $x \to \infty$, but this point has not been proved. Another limitation is that as $x \to \infty$ the edge of the wake eventually reaches the top of the boundary layer, which invalidates our analysis of § 2.2. For these reasons it is not suprising that Weighardt (1953) found that the additional drag caused by two-dimensional obstacles on a flat plate tended to a non-zero constant as the plate length was increased. However, it is not clear from the experimental results what happens as $h/\delta \to 0$. Plate (1964) deduced from his own and Weighardt's (1953) experiments that for $h/\delta > 0{\cdot}09$ the net extra drag D_{bw} for a two-dimensional plate and the wall is given by

$$D_{bw} = D + \int_{-\infty}^{\infty} \tau_{xy}(y=0)\,dx = \tfrac{1}{2}\rho U^2(h)\,h\{1{\cdot}05 - 0{\cdot}105(\delta/h)^{\frac{2}{7}}\},$$

which suggests that, when h/δ is small enough, $D_{bw}/[\frac{1}{2}\rho U^2(h)\,h]$ may become small. Further experimental investigations of D_{bw} when $h/\delta \ll 1$ could perhaps elucidate this point.

The complicated form of (2.34) suggests why attempts to use the momentum integral equation to find the drag have not been successful. Seginer (1972) showed by a specific example that consistent results cannot be obtained unless (at least) all the terms of (2.34) are calculated.

Couple. The analysis of the mean velocity deficit in § 2.2 showed that the wake strength was related to a constant $\tilde{C}$, representing a component of the moment of momentum deficit:

$$\tilde{C} = -\int_0^{\infty} yU(y)\,(u - u_E)\,dy.$$

This suggests that $\tilde{C}$ is related to the couple on the body, as it is for laminar flow. With the same control volume as before, this couple is

$$\begin{aligned} C = &\int_0^Y y\{p(\overline{u}_{x_1}^2 - \overline{u}_{x_2}^2) + p_1 - p_2 - (\overline{\tau}_{xx_1} - \overline{\tau}_{xx_2})\}\,dy \\ &+ \int_0^Y \{\rho(X_1\overline{u}_{x_1}\overline{u}_{y_1} - X_2\overline{u}_{x_2}\overline{u}_{y_2}) - (X_1\overline{\tau}_{xy_1} - X_2\overline{\tau}_{xy_2})\}\,dy \\ &+ \int_{X_1}^{X_2} \{-Y\overline{u}_{x_4}\overline{u}_{y_4} + x(\rho\overline{u}_{y_4}^2 + p_4 - \overline{\tau}_{yy_4}) - xp_3\}\,dx. \end{aligned}$$

Using the results of § 2.2 and continuity the largest terms here are

$$\begin{aligned} C = -\int_0^Y &\{2yU(y)\,u(X_2,y) - YU(Y)\,u(X_2,y) - X_2U(y)\,v(X_2,y)\}\,dy \\ &+ \int_0^Y X_2\tau_{yx2}\,dy - \int_{X_1}^{X_2} xp_3\,dx. \end{aligned}$$

But, according to the approximations made in § 2.2 in the wake

$$\int_0^Y \tau_{yx}\,dy \propto \int_0^Y \frac{\partial u}{\partial y}\,dy = 0,$$

so the combined couple on the obstacle and on the surface is

$$C_{os} = C + \int_{X_1}^{X_2} x p_3\,dx = -\rho \int_0^Y \{[2yU(y) - YU(Y)]\,u - X_2\,U(y)\,v\}\,dy. \quad (2.36)$$

From the experimental results for τ_{xy} it can be confirmed that the shear stress integral is very small compared with the inertia integrals. In fact it is possible to derive a similar expression (exactly) avoiding the assumption of constant eddy viscosity, but it is more complex than is necessary here and will be discussed elsewhere (Jackson 1973). Now the experimental data of Plate (1967) and Good & Joubert (1968) on two-dimensional bluff bodies in boundary layers show that

$$\int_{X_1}^{X_2} x p_3\,dx$$

is negative and almost equal to C, so that small errors in measuring or estimating the terms on the left of (2.36) will lead to serious errors on the right. One expects

$$\int_{-\infty}^{\infty} x p_3\,dx$$

to be a fixed multiple of C for obstacles of fixed shape and size relative to δ, but this multiple can only be found by experiment. Once it is found, however, the wake strength of any given obstacle follows from (2.36).

It is possible to estimate the pressure couple by assuming that the linearization of the equations is valid everywhere. If the resulting pressure is denoted by p_l,

$$-\partial p_l/\partial y = \rho U(y)\,\partial v/\partial x$$

and so, neglecting the pressure on face 4,

$$\int_{X_1}^{X_2} x p_{l3}\,dx = \int_0^Y U(y)\left(\int_0^y u\,dy'\right)dy + \int_0^Y X_2\,U(y)\,v\,dy. \quad (2.37)$$

Subtracting this from (2.36), and integrating by parts, we define

$$\tilde{C}_{os} = C + \int_{X_1}^{X_2} x(p_3 - p_{l3})\,dx = -\rho \int_0^Y y\left[U(y)\,u - \frac{dU}{dy}\int_0^y u\,dy'\right]dy. \quad (2.38)$$

With $u = A(x)\,U'(y) + \tilde{u}(x, y)$ this becomes

$$\tilde{C}_{os} = -\rho \int_0^\infty y\left[U(y)\,\tilde{u} - \frac{dU}{dy}\int_0^y \tilde{u}\,dy'\right]dy \quad (2.39)$$

as the control volume expands. It may be shown from (2.26) that

$$\int_0^y \tilde{u}\,dy' \sim y^{-2} \quad \text{as} \quad y \to \infty,$$

so for a power-law profile

$$\tilde{C}_{os} = -\rho \frac{1+2n}{1+n} \int_0^\infty yU(y)\,\tilde{u}\,dy = \frac{1+2n}{1+n}\,\tilde{C}. \tag{2.40}$$

The significance of (2.40) is that it gives a simple relation between an integral $\tilde{C}$ of the velocity in the wake and the sum $\tilde{C}_{os}$ of the couple C on the obstacle and the difference

$$\int_{X_1}^{X_2} x(p_3 - p_{l3})\,dx$$

between the added pressure couples on the surface. Since the surface pressure p_{l3} calculated from the linearized wake equation differs from p_3 only in the near wake and in the 'bubble', it follows that $\tilde{C}$ is a measure of the pressure forces acting on the body and the surface close to the body. In other words it is an integral which relates the wake flow far from the body to the pressure field close to the body. It is not a direct relation between the wake flow and the drag or couple on the body. An examination of the velocity profiles and streamlines of Good & Joubert's (1968) experiment suggests that for all values of $x > 0$ $-p_{l3} > -p_3$, and consequently that

$$\tilde{C}_{os} > C, \quad \rho\tilde{C} > C. \tag{2.41}$$

There are flows where the effects of the added surface couples are small, the most important being the turbulent wake behind a three-dimensional body. This case was mentioned in the review by Hunt (1971*a*) and will be discussed in a later paper. Another case is turbulent flow over a two-dimensional hump where separation does not occur, and in that case $\tilde{C}_{os} = C$ (Jackson 1973).

2.4. *Calculation of Reynolds stress and turbulent velocities*

Reynolds stress. In the wake the perturbation Reynolds stress is

$$\tau_{xy} = \rho\Delta(-\overline{u'_x u'_y}),$$

where u'_x and u'_y are the turbulent components of velocity in the x and y directions and $\rho\Delta(-\overline{u'_x u'_y})$ is the *increase* in Reynolds stress in the wake above that in the boundary layer. Thus our assumption (2.15) for τ_{xy} in the mixing region (M) and our assumption of a self-preserving velocity profile in (2.19) imply that

$$\frac{\Delta(-\overline{u'_x u'_y})}{U^2(h)} = \frac{\hat{u}K^{1-1/(2+n)}\,d^2f/d\eta^2}{(x/h)^{1+1/(2+n)}} \tag{2.42}$$

so in (M) a plot of $(x/h)^{(3+n)/(2+n)}\Delta(-\overline{u'_x u'_y})/U^2(h)$ against η should collapse all shear stress data from the wake onto a single curve. This curve is shown in figure 4 with the same value of $\tilde{C}$ as was used in the calculation of u shown in figure 2. In particular the maximum increase in Reynolds stress in (M) is given by the expression

$$\frac{\Delta(-\overline{u'_x u'_y})_{\max}}{\hat{u}U^2(h)} = \frac{K^{(1+n)/(2+n)}\,0{\cdot}88}{(x/h)^{(3+n)/(2+n)}} \quad (>0). \tag{2.43}$$

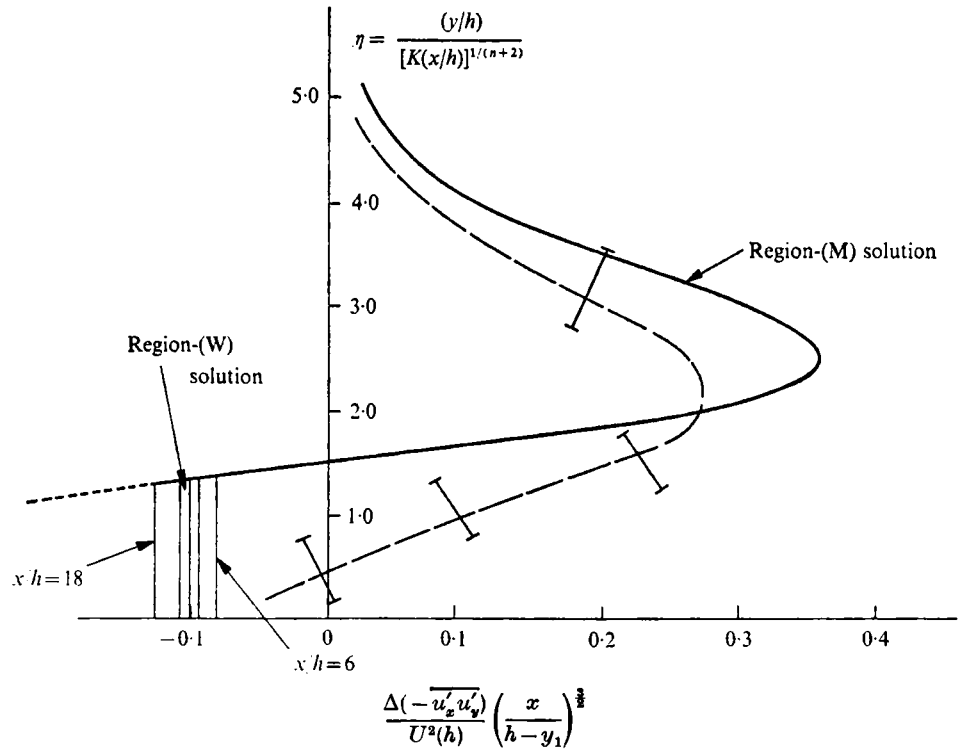

FIGURE 4. Self-preserving profiles of the perturbation Reynolds stress behind a two-dimensional obstacle. —⊥—, experimental curve with scatter bar ($n = 0{\cdot}125$, $h/\delta = \frac{1}{8}$); ——, theoretical curve deduced from the theoretical velocity profile.

Thus the maximum Reynolds stress in the main part of the wake is *greater* than the Reynolds stress upstream, although the velocity is less. The behaviour of $\Delta(-\overline{u'_x u'_y})$ in the wall region (W) is quite different. It follows from (2.33*b*) that

$$\frac{\Delta(-\overline{u'_x u'_y})}{\hat{u}U(h)\,U_*} \simeq -\left\{\frac{2\kappa f'(\eta_0)}{\ln[(\eta_0 l - y_1)/y_0]}\right\}\frac{1}{x/h}. \tag{2.44}$$

Thus in (W) the Reynolds stress is *decreased* and, it is interesting to note, this decrease extends further downstream than the increase in Reynolds stress in the mixing region; the *decrease* falls off approximately like $(x/h)^{-1}$ whereas the increase falls off approximately like $(x/h)^{-\frac{3}{2}}$. This difference in the behaviour of $\Delta(-\overline{u'_x u'_y})$ in regions (M) and (W) means that a similarity plot is not possible for both regions. Thus the graph of $\Delta(-\overline{u'_x u'_y})$ shown in figure 4 is a universal plot for region (M) but not for region (W). Note that Townsend's (1965) theory predicts that the Reynolds stress everywhere falls off with distance approximately as $(x/h)^{-1}$.

Turbulent velocities. The theoretical and experimental study of many types of turbulent shear flow has shown that in self-preserving and equilibrium flows the maximum mean-square turbulent velocities are proportional to the maximum Reynolds stress. If we make that assumption for these wake flows it follows

that the changes in the mean-square turbulent velocities in the x and y directions are given by

$$\left.\begin{aligned}\Delta\overline{(u_x')^2} &= \lambda_1 \Delta(-\overline{u_x' u_y'}),\\ \Delta\overline{(u_y')^2} &= \lambda_2 \Delta(-\overline{u_x' u_y'}).\end{aligned}\right\} \tag{2.45}$$

Taking values of λ typical of the atmospheric boundary layer ($\lambda_1 \simeq 5$, $\lambda_2 \simeq 1{\cdot}5$), it follows from (2.43) that in (M) the maximum increases in mean-square turbulent velocities are given by

$$\left.\begin{aligned}\frac{\Delta\overline{(u_x')^2_{\max}}}{U^2(h)} &\simeq \frac{10{\cdot}4K^{(1+n)/(2+n)}}{(x/h)^{(3+n)/(2+n)}},\\ \frac{\Delta\overline{(u_y')^2_{\max}}}{U^2(h)} &\simeq \frac{3{\cdot}0K^{(1+n)/(2+n)}}{(x/h)^{(3+n)/(2+n)}}.\end{aligned}\right\} \tag{2.46}$$

It might be expected that in the wall region, where the shear stress is reduced, $\Delta\overline{(u_x')^2}$ should be reduced also. This is an oversimplified prediction because the large turbulent eddies in the mixing region (M) can induce irrotational fluctuating velocities near the wall. The balance between these two effects is difficult to predict by a simple theory.

3. Wind-tunnel experiments on a wake behind a two-dimensional block

3.1. *Experimental results*

There are two methods of generating boundary layers in a wind tunnel sufficiently thick for investigating the flow over obstacles on the surface which are small compared with the boundary-layer thickness δ. The natural method is to allow the boundary layer to develop naturally along a wall of the wind tunnel, but in order that the boundary-layer thickness be great enough an unusually long wind tunnel is required. A number of such tunnels have now been constructed, the one at Colorado State University having been used successfully by Plate & Lin (1965) to examine some aspects of the flow over obstacles placed on a smooth wall. The alternative method is to create a thick fully developed layer in a short tunnel distance by using fences and other deflecting devices. Various artificial methods of simulating the atmospheric boundary layer have been developed in recent years. The experiments we shall describe were performed in the simulated boundary layer developed at C.E.R.L. by Counihan (1969). As shown in figure 5, the installation consists of a castellated fence producing a momentum defect near the wall, followed by a row of 'vorticity generators', which are wedge shaped in plan and quarter-ellipses in side view. The purpose of these generators is to create the large-scale turbulence found in the natural boundary layer and to extract momentum from the outer part of the boundary layer. The method has been used both in the small tunnel used in these experiments (618 × 185 mm in cross-section) and in a large tunnel (153 × 4·58 m), and has been shown to model most aspects of the turbulent boundary layer satisfactorily over a limited range of the tunnel. In these experiments the hot-wire probe was fixed at 686 mm, or 4·5 boundary-layer heights, downstream of the vorticity generators and the

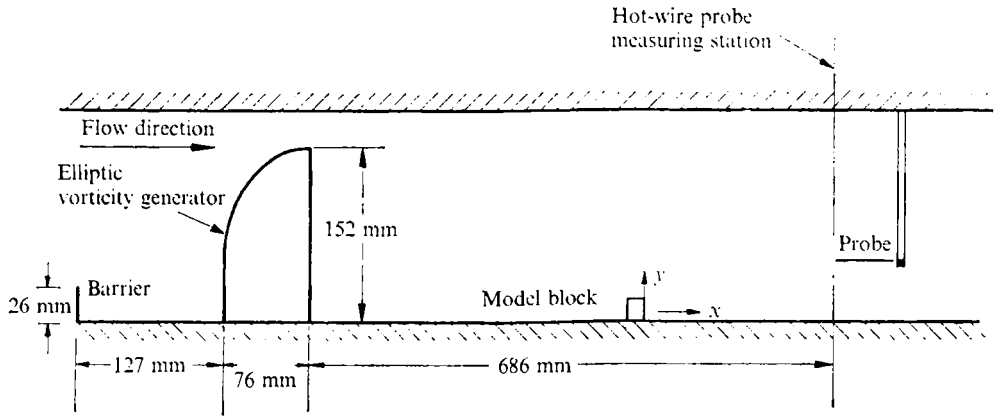

FIGURE 5. Layout of the C.E.R.L. boundary-layer wind-tunnel working section.

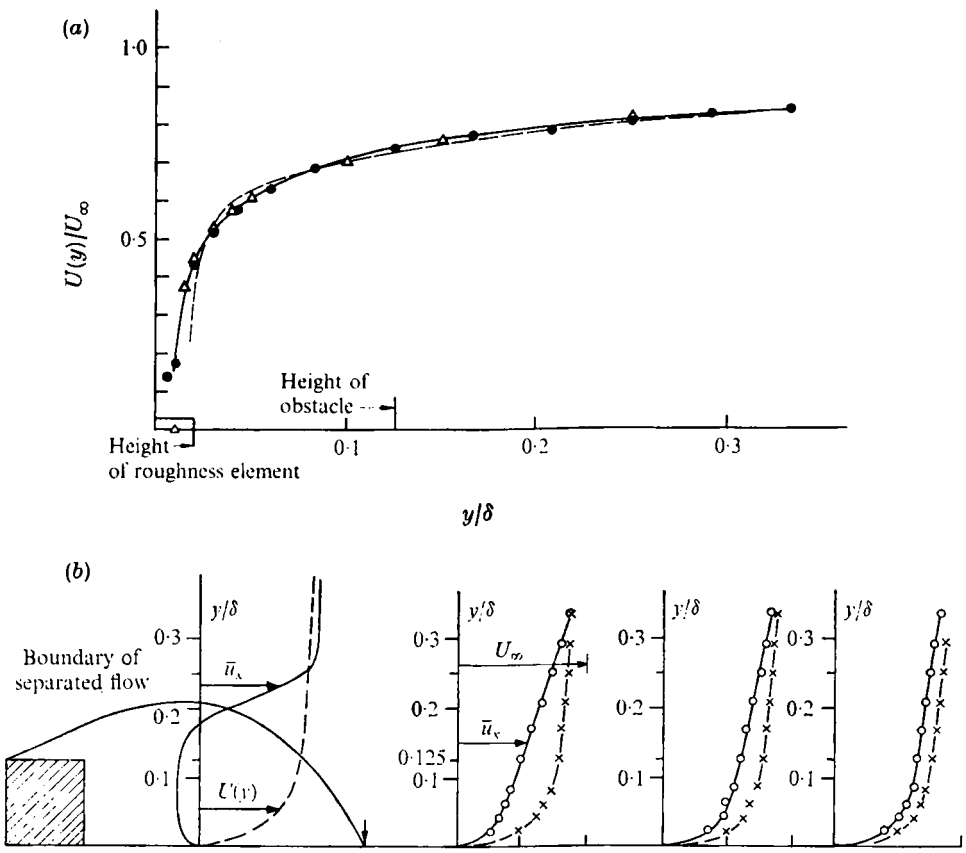

FIGURE 6. (*a*) Comparison of the boundary-layer profile $U(y)$ with power-law and logarithmic-law representation. —●—●—, measured profile; — — —, power law; △, points calculated from logarithmic law. (*b*) Measurements of the mean velocity in the wake of a two-dimensional block. Velocity profile at $x/h = 3$ is a sketch based on approximate measurements and flow visualization.

obstacle was then placed at various distances upstream of the probe. This was unsatisfactory because the boundary layer was still developing, so that the flow over the block was not always the same. However, the flow was measured with and without the obstacle so the errors in the wake should be small.

The velocity profile near $y = 0$ at the position of the probe is shown in figure 6 (a), as well as the best power-law and logarithmic profiles for comparison with the assumed profile of (2.2). By expressing the results in terms of a free-stream speed and a nominal δ, the best power-law fit was found to be

$$U(y)/U_\infty = 0{\cdot}965(y/\delta - 0{\cdot}02)^{0{\cdot}125}, \tag{3.1}$$

and the best logarithmic law

$$\frac{U(y)}{U_\infty} = 0{\cdot}125 \ln\left[\frac{y/\delta - 0{\cdot}01}{0{\cdot}0003}\right]. \tag{3.2}$$

When these two curves in figure 6 (a) are compared it is clear that the logarithmic law is marginally a better fit as y approaches the height k of the roughness elements ($k/\delta = 0{\cdot}02$). This form of the logarithmic law also agrees with the measured Reynolds stresses: the stress at $y = 0$ was found to be such that $U_* = 0{\cdot}115\kappa U_\infty$ and the stress was appreciably constant near $y = 0$, only varying by 10 % from $y = 0$ to $y = \frac{1}{6}\delta$.

The two-dimensional block used had a square cross-section and height $h = 19$ mm. Thus $h/\delta = \frac{1}{8}$ and $h/k \simeq 11$, which satisfies the first restriction of the theory, equation (2.1). Flow visualization in the boundary layer revealed that separation occurred off the top upstream edge and reattachment at about $x/h \simeq 6$. Thus, for $0 < x/h < 6$, reverse flow occurred in the wake and so the hot wire could not be used in this region, as sketched in figure 6 (b). Hot-wire measurements of the mean velocity profile $\overline{u}_x(y)/U_1$ at various stations downstream of the body in the wake for $x/h > 6$ are also shown in figure 6 (b). In figures 7 (a) and (b), $(\overline{(u'_x)^2})^{\frac{1}{2}}/U(h)$ and $(\overline{(u'_y)^2})^{\frac{1}{2}}/U(h)$ are plotted as functions of y/h at various positions in the wake. The general features of these results are predictable, namely that the velocity defect $-u$ and the additional turbulence decrease as x/h increases; the position of the maximum value of $-u$ occurs at a value of y which increases as x/h increases. Also the position of the maximum intensity of turbulence occurs at values of $y > h$, which suggests that this intense turbulence emanates from the shear layer trailing from the top of the body.

3.2. *Comparison of experiments with theory*

The first test for the theory proposed in § 2 must be whether the experimental profiles of $u(y)$ are self-preserving and can be plotted on a single curve. Therefore in figure 8 our experimental values of $(u/U(h))\,x/(h-y_1)$ are plotted against $\eta = [y/(h-y_1)]/[Kx/(h-y_1)]^{1/(n+2)}$, where $n = \frac{1}{8}$ and from (3.2) and (2.19b) $K = 0{\cdot}05$. The figure shows that this method of plotting leads to the results for $21{\cdot}1 > x/(h-y_1) > 7{\cdot}5$ being scattered around a single curve, but with no discernible systematic deviation. A 'best' experimental curve has been drawn and this is the curve which was compared with the theory in figure 2. Note

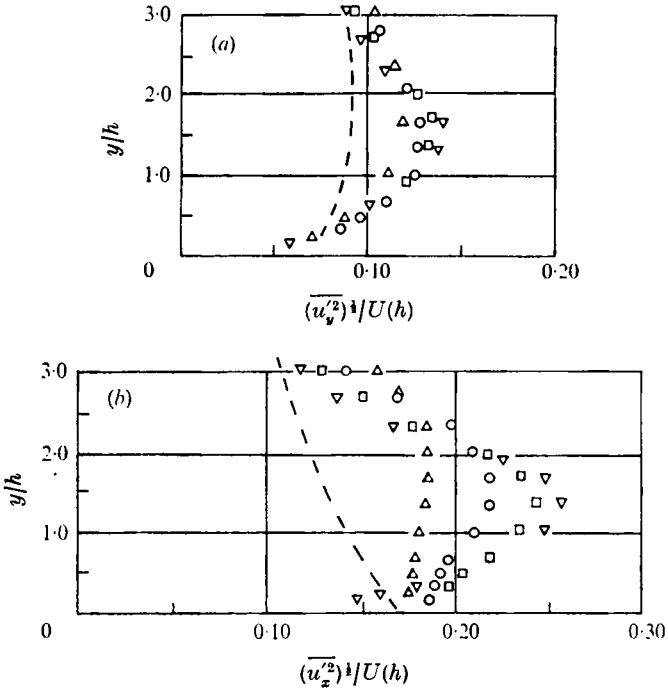

FIGURE 7. R.m.s. longitudinal and vertical turbulent velocity components in the wake of a two-dimensional block. x/h: ▽, 6·34; □, 8·84; ○, 13·5; △, 17·7. – – – –, turbulence in absence of obstacle.

that the parameter $\tilde{C}$ needed to evaluate the theoretical curve was chosen so that the maximum values of the theoretical and experimental values of $(u/U(h))x/(h-y_1)$ are the same.

Figures 2 and 8 clearly demonstrate that the profiles of u are self-preserving and that the maximum value of $u(y)$ falls off like x^{-1}. The results also show that the theoretical velocity profiles for (M) and (W) describe the measured self-preserving profiles tolerably well. The theoretical profiles show the best agreement at the top of the wake and very close to the wall, which was not unexpected from the shear stress models used in the two regions. It is also interesting that the wake is still described by the theory for values of $x/h \simeq 8$, where $u/U(h)$ is as much as 0·5, even though the theory is technically only valid if $u/U(h) \ll 1$. Note that, at this value of x/h, $n(1-n)/(l/h)^2$ is 15 times as great as $(x/h)^{-2}$, so that the assumptions for the analysis of (E) are satisfied.

An important implication of the theory for the wake is that the integral

$$\tilde{C} = \int_0^\infty yU(y)\,\tilde{u}\,dy$$

is convergent and has the same value at all positions downstream. (Note that $\tilde{u}$ is the value of u less the displacement solution $u_E(y)$ as $\eta \to \infty$, which is proportional to $(x\eta)^{-1}$.) The experiments have confirmed the theoretical distribution of the wake velocity deficit and therefore support the prediction that it is not a

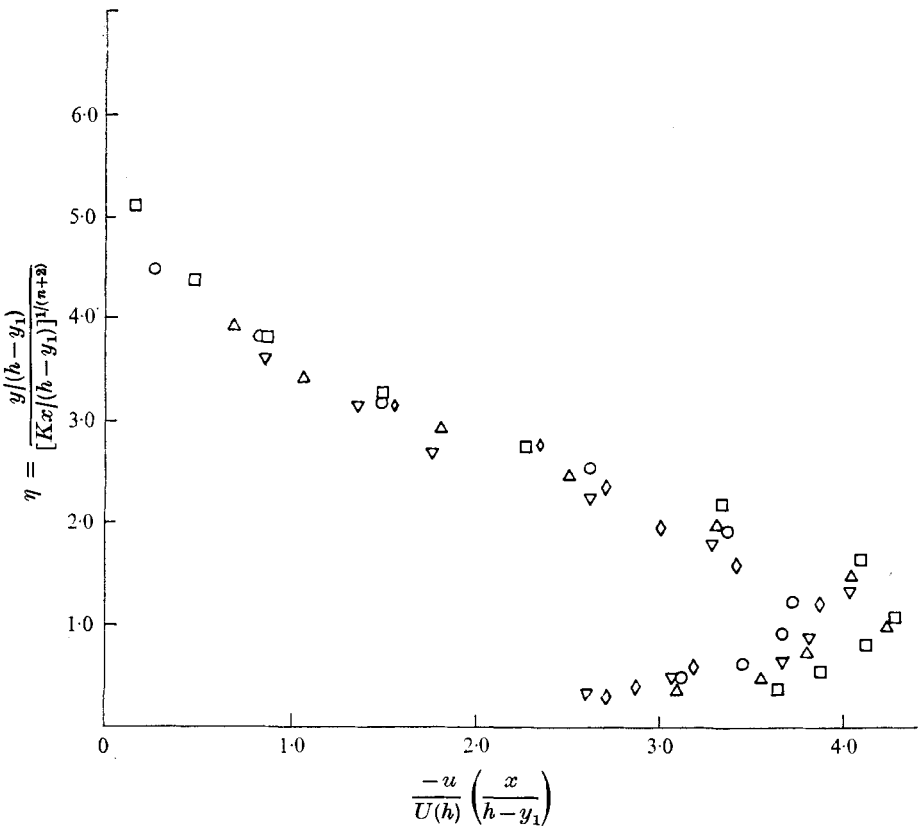

FIGURE 8. Velocity deficit measurements plotted as a self-preserving profile for the wake behind a two-dimensional block ($n = 0{\cdot}125$, $K = 0{\cdot}050$, $h/\delta = \frac{1}{8}$). $x/(h-y_1)$: ○, 7·5; □, 10·5; △, 13·0; ▽, 16·1; ◇, 21·1.

momentum integral but the moment of momentum integral $\tilde{C}$ which characterizes the wake behind a body in a boundary layer. The dimensions of $\rho\tilde{C}$ are the same as those of the couple on the body and since in § 2.3 it was argued that $\tilde{C}$ is related to C, it is interesting to compare them. In the theoretical calculations of $u/U(h)$ in figure 2 the arbitrary constant $\hat{u}$ in (2.19) was taken to be such that $u/U(h)$ agreed with the experimental results at the maximum value of $u/U(h)$. Thus

$$\hat{u} = \frac{[(u/U(h))\,x/(h-y_1)]_{\max}}{\dfrac{d}{d\eta}\left(\eta^2 M\left(\dfrac{2-n}{2+n}, \dfrac{4+n}{2+n}; \dfrac{-\eta^{n+2}}{(n+2)^2}\right)\right)_{\max}}$$

and

$$\tilde{C} = -(h-y_1)^2\,U^2(h)\,K\hat{u}I.$$

For these experiments where $n = 0{\cdot}125$ and $K = 0{\cdot}05$ $\tilde{C} = 0{\cdot}8U^2(h)\,(h-y_1)^2$.

The approximate solutions for regions (M) and (W) were earlier shown to be valid only if the parameters B and ϵ (defined by (2.24) and (2.31)) were such that $B = O(1)$ and $\epsilon \ll 1$. The data from our experiments as x increased from 7·5 to 21·0 gave the value of ϵ as changing monotonically from $-0{\cdot}11$ to $-0{\cdot}18$, and that of B as changing from 0·43 to 0·47.

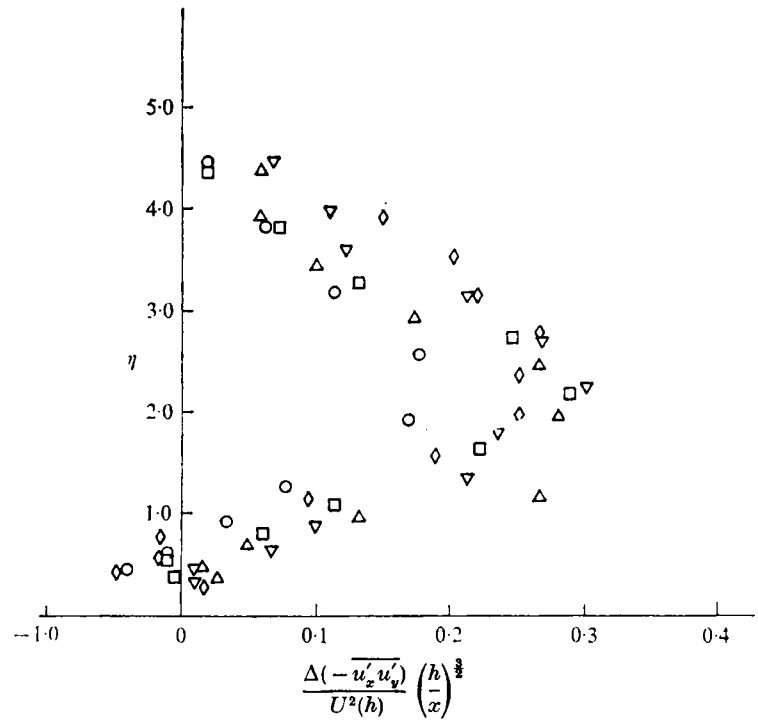

FIGURE 9. Measurements of the perturbation Reynolds stress plotted as a self-preserving profile for the wake behind a two-dimensional block ($n = 0{\cdot}125$, $K = 0{\cdot}05$, $h/\delta \simeq \frac{1}{8}$). $x/(h-y_1)$: ○, 7·5; □, 10·5; △, 13·0; ▽, 16·1; ◇, 21·1.

Neither the couple nor the pressures on the body were measured. However, from the Building Research Station Digest no. 119 (1970) for pressures on rectangular blocks in shear flows an estimate for the couple C can be made. These data give the pressure coefficients for the upstream and downstream faces as approximately uniform and equal to 0·7 and $-0{\cdot}5$, and for the upper surface near the leading edge as $-2{\cdot}0$, whence

$$C \simeq 0{\cdot}37\rho h^2 U^2(h),$$

whereas

$$\tilde{C} = 0{\cdot}8h^2U^2(h).$$

Thus the prediction of (2.41) that $\rho\tilde{C} > C$ is borne out. In fact it appears that a major contribution to $\tilde{C}$ must come from the added surface couple of the low pressure region behind the bluff body.

The next test of the theory is whether it adequately describes the shear stresses. In figure 9 we have plotted

$$\frac{\Delta(-\overline{u'_x u'_y})}{U^2(h)}\left(\frac{x}{h-y_1}\right)^{\frac{3}{2}}$$

as a function of $(y/(h-y_1))/[Kx/(h-y_1)]^{1/(n+2)}$, which confirms that the experimental profiles are self-preserving. However, the theoretical Reynolds stress profile shown in figure 4, which was obtained from the theoretical curve of $u(x, y)$

x/h	6·34	8·84	13·8	17·0	Theoretical values
$\left[\frac{\Delta\overline{(u_x')^2}}{\overline{U^2(h)}}\right]_{\max}\left(\frac{x}{h}\right)^{(3+n)/(2+n)}$	0·67	1·10	1·41	1·18	2·3
$\left[\frac{\Delta\overline{(u_y')^2}}{\overline{U^2(h)}}\right]_{\max}\left(\frac{x}{h}\right)^{(3+n)/(2+n)}$	0·18	0·24	0·41	0·46	0·7

TABLE 1. Maximum increase in turbulence in wake behind a two-dimensional model block ($n = 0{\cdot}125$)

in figure 2, has the same shape as the experimental profile and is of the same order of magnitude, but does not agree closely with the experimental profiles except as $\eta \to \infty$ and $\eta \to 0$. If the maximum slope of the *experimental* curve in figure 2 is used to calculate the maximum value of $\Delta(-\overline{u_x'u_y'})$ the agreement between the theoretical and experimental maxima is very close, but the fit still remains poor near the value of η at which u has its maximum.

From the experimental values of the two components of r.m.s. turbulent velocity in figure 7, the maximum values of

$$[\Delta\overline{(u_x')^2}/U^2(h)]\,(x/h)^{\frac{3}{2}} \quad \text{and} \quad [\Delta\overline{(u_y')^2}/U^2(h)]\,(x/h)^{\frac{3}{2}}$$

can be evaluated for comparison with the prediction of (2.46). The experiments do not provide a critical test for the theory. But the results given in table 1 below are not inconsistent with the prediction that the increase in mean-square turbulence is proportional to $(x/h)^{-\frac{3}{2}}$.

This general result should be of some practical use. The theoretically determined value for the constant of proportionality does not agree with these experimental results, but this is not surprising on account of the disagreement between the predicted and measured values of $\Delta(-\overline{u_x'u_y'})$. It is interesting that, although the shear stress at $y = 0$ is slightly less than that in the incident flow (as determined from the velocity profiles and extrapolation to $y = 0$ of the Reynolds stress measurements), the turbulent velocities are slightly greater. This suggests that the turbulent eddies from the mixing region (M) perhaps induce velocity fluctuations near the surface and if so this result supports our hypothesis that large eddies in (M) exist which share momentum and give rise to an approximately constant eddy viscosity in (M).

4. Comparison with other experiments

We now consider those experimental measurements (known to us) of flow behind two-dimensional bluff bodies in turbulent boundary layers which are sufficiently detailed to confirm or refute our theory and to compare with our experiments.

Plate & Lin (1965) measured the mean and fluctuating velocities and surface pressures behind wedge-shaped obstacles placed in turbulent boundary layers which were artificially thickened by a trip and a roughened section of the floor

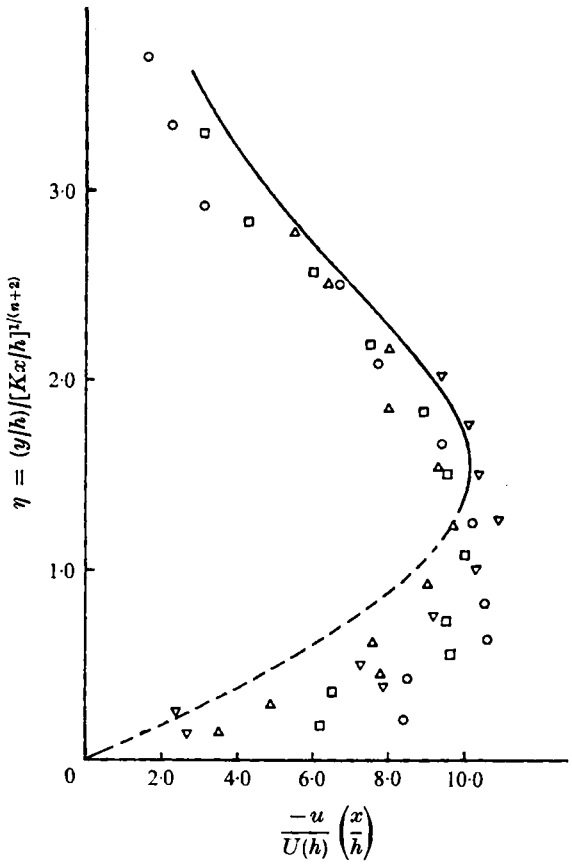

FIGURE 10. Self-preserving plot of Plate & Lin's (1965) velocity measurements behind a 25 × 100 mm wedge in a turbulent boundary layer on a smooth wall ($n = 0{\cdot}2$, $K = 0{\cdot}062$, $h/\delta \simeq \frac{1}{10}$) and the theoretical profile (matching at maximum). x/h: ○, 24; □, 32; △, 46; ▽, 72. ——, region-(M) solution; – – – –, extrapolation of (M) solution into region (W).

at the tunnel entrance, and were then allowed to develop naturally over a *smooth* floor. The cross-section of the obstacles were right triangles with the sloping face downstream. Various shapes were used but we shall only use the data from one of height 25 mm and base 100 mm. This wedge was placed in a boundary layer of thickness 250 mm, so that $h/\delta = \frac{1}{10}$. At the height of the obstacle the velocity $U(h)$ was $0{\cdot}79U_\infty$ and the friction velocity was $U_* = 0{\cdot}062U_\infty$. The value of n is found to be 0·2, and the Reynolds number for the obstacle $U(h)\,h/\nu = 1{\cdot}16 \times 10^5$. Unfortunately the velocity profile at the position of and in the absence of the wedge was not measured, the only undisturbed profiles being obtained 900 mm upstream of the obstacle. In our calculations this profile was taken as $U(y)$. Values of $[u/U(h)]\,[x/(h-y_1)]$ have been calculated from Plate & Lin's data for the 25 mm wedge and plotted as a function of $(y/h)/[Kx/h]^{1/(2+n)}$ in figure 10. As with our results this method of plotting collapses the data and thus shows that the velocity deficit in the wake has a self-preserving form. The main difference

x/h	14·25	18·25	26·25	Theoretical value
$[\Delta(\overline{u_x'})^2/U^2(h)]_{\max}$	0·036	0·029	0·016	
$\left[\frac{\Delta(\overline{u_x'})^2}{U^2(h)}\right]_{\max}\left(\frac{x}{h}\right)^{\frac{3}{2}}$	1·95	2·26	2·14	2·6

TABLE 2

between Plate & Lin's results and our experimental results is that their velocity deficit is about 2·5 times as great. This may be caused by the fact that the only measurement of the undisturbed velocity profile was taken so far upstream, but the main difference between the two experiments is that Plate & Lin used a smooth wall (with $U_*/U(h) = 0{\cdot}079$), whereas in our experiments the wake developed over a rough wall (with $U_*/U(h) = 0{\cdot}060$). There is also a difference in the Reynolds numbers of the flow over the obstacles, theirs being $1{\cdot}11 \times 10^5$ compared with only 1×10^4 in our experiments. Despite those differences, it is interesting to observe that the self-preserving velocity profile still agrees quite closely with the theoretical profile for the mixing region (M), if the disposable constant in the theoretical profile is chosen to achieve a best fit at the maximum value of u. (The solution for the wall region (W) is omitted because of the smooth surface.) Plate & Lin (1965) measured the pressure distribution along the surface behind one larger wedge. These results also show that the length of the bubble was about $10h$, and that the maximum difference between the pressure on the surface just downstream of the bubble and that far downstream was approximately $0{\cdot}08\rho U(h)\,|u_{\max}|$. This provides an excellent experimental confirmation of our analysis in § 2.2 that in the wake the perturbation pressure gradient $\partial p/\partial x$ is negligible compared with terms like $\rho U(h)\,\partial u/\partial x$. The measurements of mean-square turbulent velocities are difficult to analyse because of the lack of data on the undisturbed flow. But if values for $(\overline{u_x'})^2/U_\infty$ typical of turbulent boundary layers are used for the upstream turbulence then we find (see table 2) that the results for $\Delta(\overline{u_x'})^2_{\max}$ are similar to our experimental results. If the theory of § 2.3 is valid then, since the maximum value of $-u/U(h)$ in Plate & Lin's experiments on the 50×100 mm wedge is twice as great as those for our experiment, the predicted value of $(\Delta(\overline{u_x'})^2/U^2(h))\,(x/h)^{\frac{3}{2}}$ is twice as great also. The theoretical value is obtained as before, by choosing the constant $\hat{u}$ such that experimental and theoretical mean velocity profiles agree when $-u/U(h)$ is a maximum. The reason why the experimental values in this case also fall below the theoretical value is again that the shear stress model is inadequate.

The other set of detailed measurements contains those performed by Nageli (1953). These consisted of mean velocity profiles upwind and downwind ($x/h < 30$) of a fence 2·2 m high and 24 m long erected on flat grassland. Two different fences, both constructed with wooden slats, were used in two sets of measurements; in the first case the open-area ratio ϕ was 20 % and in the second case 50 %. From the published data $(-u/U(h))\,(x/h)$ was calculated and the results for the two fences are plotted in figures 11 (*a*) and (*b*). In each figure the experimental

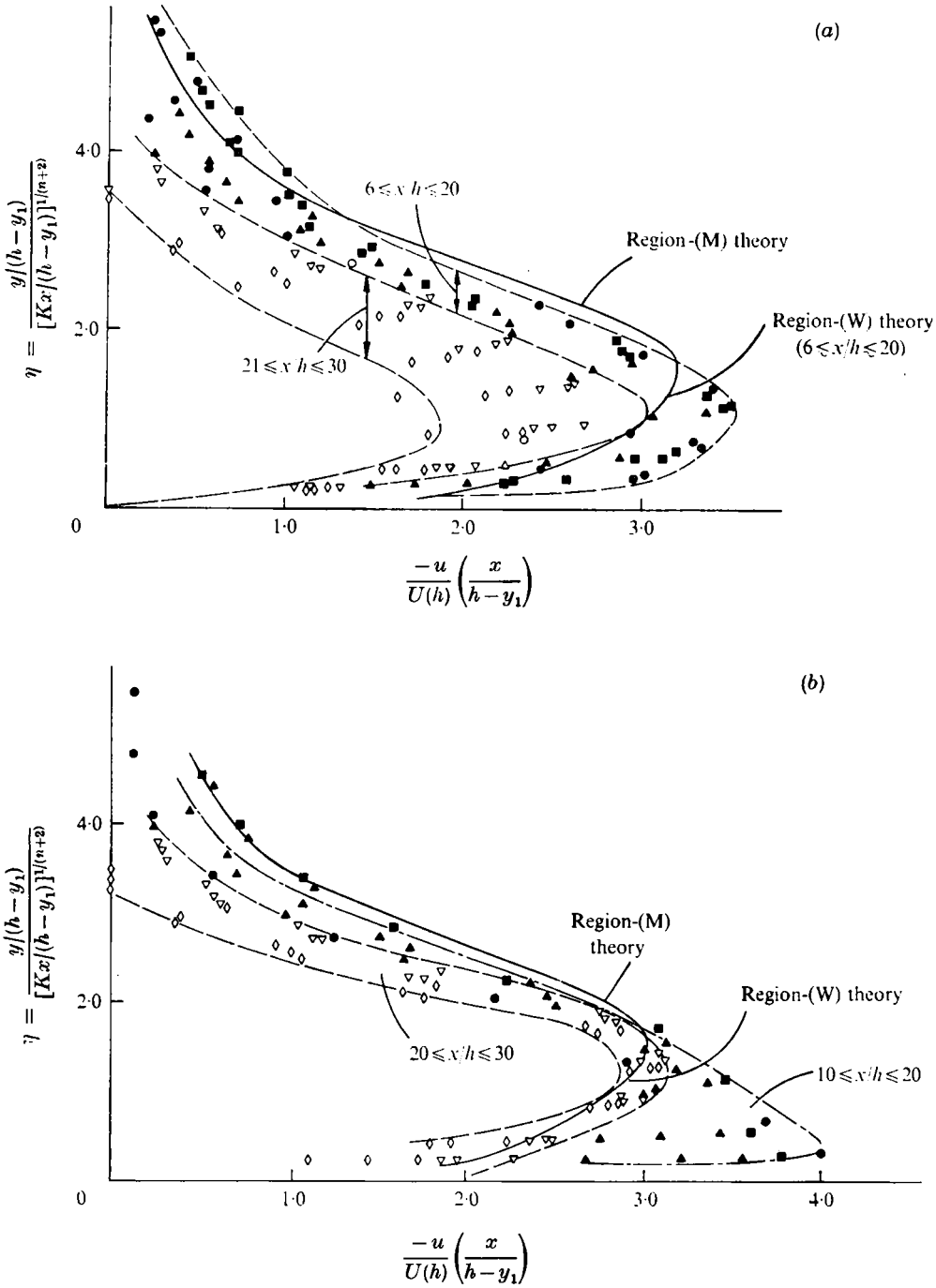

FIGURE 11. Velocity deficit measurements plotted as self-preserving profiles for the natural wind behind porous screens on grassland (Nageli 1953; $n = 0{\cdot}2$; $K = 0{\cdot}056$, $h = 2{\cdot}2$ m. breadth 24 m) and the theoretical profiles (matching at maximum). Ranges of x/h: ●, 6–10; ■, 11–15; ▲, 16–20; ▽, 21–25; ◇, 26–30. (*a*) Screen with 20% open-area ratio. (*b*) Screen with 50% open-area ratio.

results are presented in groups for two ranges of x/h. For the denser fence ($\phi = 0{\cdot}2$) the results only display a self-preserving form for $21 \geqslant x/h \geqslant 6$. For $x/h > 21$ the velocity deficit decreases more rapidly than x^{-1}, presumably because the fence is only of finite width ($11h$) and sufficiently far downstream the wake ceases to be two-dimensional. Note that the maximum value of $[-u/U(h)](x/h)$ is about 3·1, which is less than in our model experiments (4·0) but is of the same order. Since we expect that the value of $\tilde{C}$ increases with the couple, then the fact that the couple on a porous fence is lower than on a solid obstacle should explain why $\tilde{C}$ is lower in Nageli's experiments than in the model experiments.

The flow in the wake behind the more porous fence has some features quite different from those behind a solid or more dense fence. As Nageli found in his full-scale investigation and Castro (1971) and Baltaxe (1967) have found in model investigations, the recirculating bubble behind a porous fence or plate may be detached from the body. Therefore the distance downwind of the obstacle over which effective 'shelter' or reduction in wind speed occurs may be considerably greater behind a porous obstacle than a solid obstacle. This also means that behind a porous fence it takes a greater distance downwind for the perturbation velocity u to be small enough for the wake to be self-preserving. However, behind a more porous fence less lateral mixing occurs, so that the effects of the finite length of the fence are felt on the centre-line further downstream. Thus we find in figure 11 (*b*) that the wake is not self-preserving until

$$20 < x/h < 30.$$

Compared with the denser fence note that in the self-preserving region the maximum value of $[-(u/U(h))(x/h)]$, and therefore $\tilde{C}$, is *less*, although closer to the fence ($x/h < 20$) in the non-self-preserving region, $\tilde{C}$ is greater.

Since the couple C on this more porous fence is less than on the denser fence (de Bray 1971), it is interesting to note that $\tilde{C}$ is also less. On the basis of the data of Counihan's and Nageli's experiments it appears that $\tilde{C}$ increases as the couple on the body increases. The theoretical curve shown in figure 11 (*b*) has been evaluated using the same expression for eddy viscosity as is used for a solid obstacle. Since all the flow passes over a solid obstacle and forms a shear layer at the top, the height for specifying the eddy viscosity was taken as h. For a porous obstacle, since only some of the flow passes over the obstacle, it might be more logical to specify the eddy viscosity with respect to the maximum vertical distance by which streamlines are displaced, which is of order $(1-\phi)h$. This would mean that in plotting Nageli's data K would be reduced and therefore the data points in figure 11 (*b*) could be displaced upwards to agree more closely with the theoretical profile. This is only a tentative hypothesis which ought to be tested in detail.

Other data exist on wakes behind bodies in boundary layers, both full scale and model scale, but most are incomplete. However, it is often possible to extract the value of $[-u/U(h)]_{\max}$ as a function of x/h and therefore in figure 12 we compared the values for a number of experiments. The additional full-scale data are those of Rider (1952), who measured the mean wind velocity behind a hedge on a flat grass field. Since Rider only made velocity measurements at three

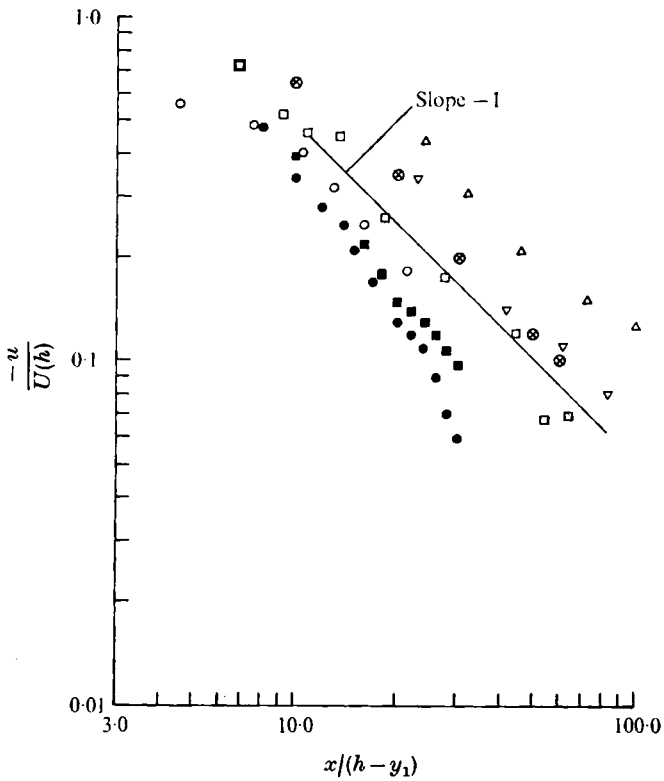

FIGURE 12. Comparison of results from several experiments for the maximum value of the velocity deficit in wakes behind two-dimensional surface obstacles as a function of the distance downstream. Rough surface: ■, thin screen, Nageli; ●, thick screen, Nageli; ○, rectangular block ($h/\delta = \frac{1}{8}$), Counihan; □, hedge, Rider. Smooth surface: △, wedge 25 × 100 mm, Plate & Lin; ▽, 50 × 100 mm, Plate & Lin; ⊗, fence, Sforza & Mons.

heights, these are insufficient to evaluate $[u/U(h)]_{\max}$. However, by assuming the theoretical velocity distributions of § 2.2, $[u/U(h)]_{\max}$ can be estimated by interpolating between the measurements. The results are shown in figure 12 and once again the x^{-1} hypothesis is supported.

Taking the results for $[u/U(h)]_{\max}$ for the wakes on rough walls measured by Counihan, Nageli and Rider, we conclude that

$$[u/U(h)]_{\max} = m(x/(h-y_1))^{-1}, \tag{4.1}$$

where m is a dimensionless constant which depends on the shape and porosity of the obstacle and also the dimensionless ratios $U(h)/U_*$, h/δ and h/k. For these three sets of experiments, which cover a considerable range of values for h/k and porosity, it is interesting that

$$3{\cdot}0 < m < 4{\cdot}0. \tag{4.2}$$

We cannot evaluate m from our theory, but we can suggest how the strength of the wake varies with the roughness of the surface. From (2.26) and (2.19b) it follows that

$$m = \frac{\tilde{C}1{\cdot}84}{K(h-y_1)^2\,U^2(h)\,I(n)} = \left[\frac{\tilde{C}}{(h-y_1)^2\,U^2(h)}\right]\frac{1{\cdot}84\ln\left((h-y_1)/y_0\right)}{I(n)\,2\kappa^2}. \tag{4.3}$$

We have argued in § 2.3 that $\tilde{C}$ is primarily determined by the pressure field close to the body. Therefore, if we make the hypothesis that this pressure field is primarily determined by $U(h)$, then whatever the roughness, for a given shape and porosity,

$$\tilde{C}/[(h-y_1)^2\,U^2(h)] \simeq \text{constant}.$$

In fact the measurements of Jensen & Franck (1965) indicate that for the couple $C/[(h-y_1)^2\,U^2(h)]$ decreases as the roughness increases. We showed in § 2.2 that $I(n)$ is relatively insensitive to the value of n, varying by about 15 % over the values of n found for the smoothest to the roughest surfaces. The primary effect of roughness is to alter the eddy-viscosity expression K defined in (2.19*b*), so that from (4.1) and (4.3) we expect that

$$m \propto \ln[(h-y_1)/y_0]. \tag{4.4}$$

The W.M.O. review (van Eimern *et al.* 1964) describes a number of empirical formulae for the shelter effect. Some research has shown that $\ln[(h-y_1)/y_0]$ is a relevant parameter, but no formula such as (4.3) has been derived, even empirically. The data shown in figure 12 cannot be used to test (4.3) because each obstacle was different, but some natural and wind-tunnel measurements behind shelter belts by Jensen (1954) can be used. In the first case a natural shelter belt 3·5 m high in rough terrain ($h/y_0 = 78$) was compared with a wind-tunnel test behind a shelter belt with the same porosity (38 %) and approximately the same roughness ($h/y_0 = 56$). At twenty h downstream ($x/h = 20$), the measurements taken at $y/h = 0{\cdot}4$ give the same value of $-u_{\max}/U(h) = 0{\cdot}28$. (This incidentally was an interesting verification of the similarity of natural and wind-tunnel flows despite a huge difference in Reynolds number between the two flows.) To discern the effects of varying the roughness, measurements behind the *same* model shelter belt were then made on a much smoother surface, which was still aerodynamically rough ($h/y_0 = 4500$). In this case it was found that $-u_{\max}/U(h) = 0{\cdot}49$. If our interpretation of (4.3) is correct, then from (4.4), the ratio of $-u_{\max}/U(h)$ for these two cases examined by Jensen should be

$$\ln 78/\ln 4500 = 0{\cdot}52;$$

the experimental value for this ratio is 0·57. Another set of measurements was made behind a more porous fence (45 %) 2·5 m high on very smooth mud flats ($h/y_0 = 14\,000$), and compared with wind-tunnel tests behind model shelter belts over surfaces with two roughness lengths ($h/y_0 = 56$ and 4500). At $x/h > 25$ the ratios of the values of $-u_{\max}/U(h)$ for the rough and smooth surfaces was again approximately equal to the ratios of $\ln(h/y_0)$. Whether or not our specific hypothesis is correct, it seems likely that $-u_{\max}/U(h)$ or m decreases as the roughness of the terrain increases.

For wakes over smooth walls we have plotted Plate & Lin's (1965) results for both the 25×100 mm wedge and also the 50×100 mm wedge. We have already commented on the values of these velocity deficits being much greater than those measured on rough surfaces. Other wake measurements over smooth walls have been made by Plate (1967) behind various fences with heights much less than that of the boundary layer. From the scanty velocity measurements published

in the latter paper one finds that the values of $u/U(h)$ fall close to the values for the wakes behind the larger of the wedges of Plate & Lin.

For comparison with Plate & Lin's data for wakes on a smooth wall we have plotted the results of Sforza & Mons (1970) for the maximum velocity defect behind a fence placed at the *leading edge* of a smooth flat plate, the defect being defined as the difference between the measured velocity and that in the boundary layer on the plate in the absence of the fence, and $U(h)$ being the velocity of the free stream approaching flat plate. Although this is an entirely different type of wall wake from that which we have considered, it is noteworthy that, as Sforza & Mons remarked, their velocity defect had an $(x/h)^{-1}$ decay behaviour. It is also interesting to note that their results for $[-u/U(h)]_{\max}$ are of the same order of magnitude as those for Plate & Lin's experiments.

The similarity of all these results indicates that in turbulent wakes behind bluff obstacles placed on rough or smooth surfaces the maximum velocity deficit falls off like $(x/h)^{-1}$.

5. Conclusion

5.1. *Limitations of theory and experimental data*

The first conclusion of this paper is that a simple eddy-viscosity theory can describe most of the salient characteristics of the wake behind two-dimensional surface obstacles in turbulent boundary layers. The main shortcoming of the theory is that it does not adequately describe the distribution of shear stress and turbulent intensity across the wake, although it does suggest the dependence with distance downstream of the maximum shear stress and turbulence intensity. By considering a control surface taken around the obstacle and the structure of the wake, we have been able to show how the wake is related to the pressure field close to the body, and that for a general two-dimensional obstacle there is no simple relation between the drag or couple on the obstacle and the wake flow. Despite some success in describing these wakes, the theory is in a very primitive stage and, we believe, needs further development.

In addition to further theoretical work this wake model requires more experimental investigation both in wind tunnels and in full-scale experiments. The effects of varying the ratio h/δ for $h/\delta < 1$, the roughness of the boundary layer, and the shape and porosity of the obstacle in particular need to be investigated. When such experiments are undertaken it is most important that Reynolds stresses, turbulence intensity and if possible the turbulence scale be measured as well as the mean velocity profiles. Pressure distributions on the obstacle and the surface should be measured to test their relation with the wake flow. Vortex shedding from any surface obstacle in or outside a shear layer has hardly been measured at all, and is another aspect of the wake flow which needs to be investigated. It is of particular importance that several velocity and stress profiles should be taken in the absence of the body so that *changes* in velocity and shear stress can be calculated; it is the changes in these quantities which can be understood theoretically.

5.2. *Some practical conclusions*

We have mentioned in the introduction that an important application of the study of the wakes behind two-dimensional surface obstacles is to the design of shelter belts and windbreaks. The effectiveness of a shelter belt is often measured by the shelter parameter s, which in our notation is defined as

$$s = -u/U(y). \tag{5.1}$$

In the mixing region (M) of the wake u does not vary with y in the same way as the incident profile $U(y)$, so that s is a function of y. But in the lower part of the wall region (W), which is the relevant region for assessing the effectiveness of a shelter belt, both u and $U(y)$ are proportional to $\ln y$ [(2.3) and (2.33)] and therefore s is approximately constant, as Jensen (1954) showed experimentally. The conclusion we reach from our theory and from our own and others' experimental results is that, for wakes behind two-dimensional obstacles on a rough surface, sufficiently far downstream

$$s \simeq m/(x/h), \tag{5.2}$$

where m varies with the shape and porosity of the obstacle, and also the roughness of the surface. For a given obstacle, there are theoretical grounds for postulating that

$$m \propto \ln [(h-y_1)/y_0]$$

and a little experimental evidence of Jensen (1954) to support the hypothesis. The range of m for different types of obstacle and of terrain roughnesses lies between 3 and 10.

At distances less than $20h$ downwind the shelter depends critically on the nature of the shelter belt. The formula (5.2) would appear to be a useful approximation for dense shelter belts when $x/h > 10$, but for less dense shelter belts only when $x/h > 20$. These are tentative criteria which need further investigation. But they are at least quantitative hypotheses, which in our submission have been lacking in the past.

The increase or decrease in turbulence in the wall region (W) is also an important measure of the effectiveness of a shelter belt. A dense shelter belt produces a considerable increase in turbulence in the mixing region (M), but in (W) there is only a slight increase downstream of the bubble. The qualitative measurements of turbulence behind model porous fences by Baltaxe (1967) suggest that the more porous the fence the less the increase in turbulence. The effect of porosity is another aspect needing more experimental study.

Since $u(y)$ is proportional to $\ln y/(x/h)$ in the lower part of the wall region (W), the perturbation shear stress at the surface

$$-(\tau_{xy})_{y=0} \propto (x/h)^{-1}$$

and therefore it might be expected that this would give a measure of the reduction in heat and mass transfer far downstream in the wake.

The results of our theoretical and experimental investigations should also be of some use in assessing the effect of a building on the wind forces on another

building downwind, on the behaviour of an aircraft downwind and on the downwind dispersal of airborne pollution. Since few buildings have the shape considered in this paper our results are not as directly relevant as for shelter belts. The salient facts are that the maximum reduction in wind velocity u is proportional to $(x/h)^{-1}$ and that the vertical displacement of the position of maximum velocity deficit is approximately proportional to $(x/h)^{\frac{1}{2}}$. It may also be useful to know that the maximum increase in mean-square turbulence, which occurs at a position above the position of maximum velocity deficit, decreases approximately as $(x/h)^{-\frac{3}{2}}$. We find that, downstream of the bubble, $\Delta(\overline{u_x'})^2$ is of the same order as the upstream value of $(\overline{u_x'})^2$ even though $-u \ll U$. Thus the root-mean-square turbulence intensity $(\Delta(\overline{u_x'})^2)^{\frac{1}{2}}/U(h)$ decreases more slowly than $u/U(h)$.

This work was begun by J. C. R. Hunt and J. Counihan at the Central Electricity Research Laboratories, Leatherhead. P. S. Jackson acknowledges support from a Commonwealth Scholarship. J. Counihan acknowledges the permission of the Central Electricity Generating Board to publish this paper.

REFERENCES

Abramowitz, M. & Stegun, I. 1964 *Handbook of Mathematical Functions.* Washington: Nat. Bur. Stand.

Baltaxe, R. 1967 Air flow patterns in the lee of model windbreaks. *Arch. Met. Geophys. & Biok.* B **15**, 287–312.

Bradshaw, P. 1971 Variations on a theme of Prandtl. *AGARD Conf. on Turbulent Shear Flows, London.*

Bradshaw, P. & Wong, F. Y. F. 1972 The reattachment and relaxation of a turbulent shear layer. *J. Fluid Mech.* **52**, 113–135.

Bradshaw, P., Ferriss, D. H. & Atwell, N. P. 1967 Calculation of boundary-layer development using the turbulent energy equation. *J. Fluid Mech.* **28**, 593–616.

Bray, R. G. de 1971 Protection by fences. *Wind Effects on Buildings & Structures Seminar, University of Auckland.*

Burnham, J. 1967 A note on the turbulence problem associated with take-off and landing. *R.A.E. Tech. Rep.* no. 67240.

Castro, I. P. 1971 Wake characteristics of two-dimensional perforated plates normal to an air-stream. *J. Fluid Mech.* **46**, 599.

Counihan, J. 1969 An improved method of simulating an atmospheric boundary layer in a wind tunnel. *Atmos. Environ.* **3**, 197.

Eimern, J. van, Karschon, K., Razumora, L. A. & Robertson, G. W. (eds.) 1964 Windbreaks and shelter belts. *World Met. Office. Tech. Note*, no. 59.

Gartshore, I. S. 1972 The interaction between turbulent wakes and boundary layer flows. *Can. Aero. Space Inst. Trans.* **5**, 49.

Good, M. C. & Joubert, P. N. 1968 The form drag of two-dimensional bluff-plates immersed in turbulent boundary layers. *J. Fluid Mech.* **31**, 547–582.

Hunt, J. C. R. 1971*a* The effect of single buildings and structures. *Phil. Trans.* A **269**, 457–467.

Hunt, J. C. R. 1971*b* A theory for the laminar wake of a two-dimensional body in a boundary layer. *J. Fluid Mech.* **49**, 159.

Jackson, P. S. 1973 Flow around obstacles in boundary layers. Ph.D. thesis, Cambridge University.

Jensen, M. 1954 *Shelter Effect.* Copenhagen: Danish Technical Press.

JENSEN, M. & FRANCK, N. 1965 *Model Scale Tests in Turbulent Wind*. II. Copenhagen: Danish Technical Press.

KAISER, H. 1959 Die Strömung an Windschutzstreifen. *Berichte Deutschen Wetterd, U*, no. 53.

LAUNDER, B. J. & SPALDING, D. B. 1972 *Mathematical Models of Turbulence*. Academic.

MAIR, W. A. & MAULL, D. J. 1971 Aerodynamic behaviour of bodies in the wakes of other bodies. *Phil. Trans.* A **269**, 425–437.

NAGELI, W. VON 1953 Untersuchungen über die Windverhältnisse im Bereich von schilfrohrwänden. *Miteil, Schweiz, Anstalt, Forstl Versuchswesen, Zurich*, **29**, 213–266.

PLATE, E. J. 1964 The drag on a smooth plate with a fence immersed in its turbulent boundary layer. *A.S.M.E. Paper*, no. 64-FE-17.

PLATE, E. J. 1967 Diffusion from a ground level line source into the disturbed boundary layer far downstream from a fence. *Int. J. Heat Mass Transfer*, **10**, 181–194.

PLATE, E. J. 1971*a* Aerodynamics of shelter belts. *Aric. Met.* **8**, 203–222.

PLATE, E. J. 1971*b* Aerodynamic characteristics of atmospheric boundary layers. *U.S. Atomic Energy Comm. Crit. Rev. Ser.*

PLATE, E. J. & LIN, C. Y. 1965 The velocity field downstream from a two-dimensional model hill. *Colorado State University Rep.* CER 65 EJP 14.

RIDER, N. E. 1952 The effect of a hedge on the flow of air. *Quart. J. Roy. Met. Soc.* **78**, 97–101.

SEGINER, I. 1972 Windbreak drag calculated from the horizontal velocity field. *Boundary-layer Met.* **3**, 87–97.

SFORZA, P. M. & MONS, R. F. 1970 Wall wake; flow behind a leading edge obstacle. *A.I.A.A. J.* **8**, 2162–2167.

SMITH, F. T. 1973 Laminar flow over a small hump on a flat plate. *J. Fluid Mech.* **57**, 803–824.

TANI, N. 1958 On the wind tunnel test of the model shelter hedge (in Japanese with English summary). *Bull. Nat. Inst. Agric. Sci.* A, no. 6.

TOWNSEND, A. A. 1956 *The Structure of Turbulent Shear Flow*. Cambridge University Press.

TOWNSEND, A. A. 1961 Equilibrium layers and wall turbulence. *J. Fluid Mech.* **11**, 97.

TOWNSEND, A. A. 1965 Self-preserving flow inside a turbulent boundary layer. *J. Fluid Mech.* **22**, 773–797.

TOWNSEND, A. A. 1972 Flow in a deep turbulent boundary layer over a surface distorted by water waves. *J. Fluid Mech.* **55**, 719.

WEIGHHARDT, K. 1953 Erhohung des turbulenten Reihungswiderstandes durch Oberflachenstorungen. *Forschungshefte für Schiffstechnik*, **1**, 65.